Published in final edited form as:

Cancer Res. 2022 October 17; 82(20): 3718–3733. doi:10.1158/0008-5472.CAN-21-1225.

Dll1-mediated Notch signaling drives tumor cell crosstalk with cancer-associated fibroblasts to promote radioresistance in breast cancer

Ajeya Nandi[1], **Rahul Debnath**[1], **Anupma Nayak**[2], **Tsun Ki Jerrick To**[3], **Gatha Thacker**[1,7], **Megan Reilly**[1], **Sanjeev Gumber**[4], **Ilias Karagounis**[5], **Ning Li**[1], **Christopher J. Lengner**[1,6], **Malay Haldar**[3], **Alana L. Welm**[8], **M Blanco Andres**[1,6], **Christoforos Thomas**[5], **Rumela Chakrabarti**[1,6,7,*]

[1]Department of Biomedical Sciences, University of Pennsylvania, Philadelphia, PA 19104

[2]Department of Pathology and Laboratory Medicine, Perelman School of Medicine, University of Pennsylvania Philadelphia, Pennsylvania, PA 19104

[3]Department of Pathology and Laboratory Medicine, Perelman School of Medicine, University of Pennsylvania, PA 19104-6160

[4]Department of Pathology and Laboratory Medicine, Emory University, School of Medicine, Atlanta, GA 30329

[5]Department of Radiation Oncology, Perelman School of Medicine, University of Pennsylvania, Philadelphia, PA 19104

[6]Institute for Regenerative Medicine, University of Pennsylvania, Philadelphia, PA 19104

[7]Department of Surgery, Miller School of Medicine, Sylvester Comprehensive Cancer Center, Miami, FL 33136, USA

[8]Department of Oncological Sciences, Huntsman Cancer Institute, University of Utah, Salt Lake City, UT 84112

Abstract

Resistance to radiotherapy is a major obstacle for effective cancer treatment. Both cancer-associated fibroblasts (CAF) within the tumor microenvironment (TME) and Notch signaling are implicated in radioresistance, but their potential interrelationship is unclear. Here, we report that

*Corresponding Author Rumela Chakrabarti, PhD, Department of Surgery, Miller School of Medicine, Sylvester Comprehensive Cancer Center, Room 508, Biomedical Research Building, 1501 NW 10th Avenue, 5th Floor, Miami, FL 33136, Office phone: 305-243-6545, Cell:3303891943, rxc1335@med.miami.edu.

Author's contributions

A.N. and R.C. conceived the study and designed all experiments. A.N., R.D., G.T. and M.E.R. performed all the experiments. A.N. and R.C. analyzed the data and wrote the manuscript. A. Nayak (human) and S.G. (mouse) performed histopathological evaluation in the manuscript. C.T., I.K., C.J.L. and N.L. provided technical assistances for radiation and helpful discussions. T.K.J.T. and M.H. performed all single cell RNA sequencing data analyses. A.L.W. provided Patient derived Xenografts (PDXs) and helpful discussions. A.M.B. performed METABRIC data analyses. All authors discussed the results and commented on the manuscript.

Conflict of Interest: Authors declare no conflicts to disclose

Authors' Disclosures

No disclosures were reported by authors. University of Utah may license the HCI PDX models described herein to for-profit companies, which may result in tangible property royalties to A.L.W.

irradiated samples obtained from luminal breast cancer patient tumors express higher levels of the Notch ligand Dll1 and have a greater number of αSMA- and FAP-expressing activated CAFs. Single cell transcriptomic profiles further revealed enrichment of an αSMA$^+$ myofibroblastic subpopulation of CAF in Dll1$^+$ tumors. In murine and human PDX models, Dll1$^+$ tumor cells were more radioresistant than Dll1$^-$ tumor cells, and genetic and pharmacological blocking of Dll1-mediated Notch signaling decreased the number of Dll1$^+$ cancer stem cells (CSC) and CAFs and increased Dll1$^+$ tumor cell radiosensitivity. Dll1$^+$ cells recruited CAFs in an IL-6-dependent fashion and promoted Wnt ligand secretion by Notch2/3-expressing CAFs, thereby driving Wnt/β-catenin-dependent increases in Dll1$^+$ CSC function to promote metastasis. Treatment with the porcupine inhibitor LGK-974 that inhibits Wnt ligand secretion or pharmacological blockade of IL-6 or Dll1 suppressed CAF-dependent enhancement of Dll1$^+$ CSC function and metastasis in radioresistant tumors. Together, these findings reveal an essential crosstalk between Dll1$^+$ cancer cells and CAFs that promotes metastasis and radioresistance, which could be therapeutically exploited to improve the outcome of breast cancer patients.

One sentence summary:

Dll1 expression on tumor cells drives Notch-activated Wnt secretion by CAFs to promote radioresistance in breast cancer.

Keywords

Cancer associated fibroblast (CAF); cancer stem cell (CSC); Delta like 1 (Dll1); radioresistant breast cancer; Tumor microenvironment (TME); Disseminated tumor cells (DTCs); metastasis

Introduction

Breast cancer remains a major cause of cancer-associated death in women, despite attempts to provide effective therapies. In addition to surgery and chemotherapy, radiotherapy (RT) remains a critical component for achieving loco-regional control in breast cancer patients [1]. Prior meta-analyses demonstrated the pivotal role of RT in reducing recurrence and enhancing survival of cancer patients, while having a limited impact on their quality of life [2]. Unfortunately, a subset of patients does not benefit from RT, due to either intrinsic or de novo radioresistance, as evidenced by distant metastatic spread and local recurrence [3, 4]. Therefore, understanding mechanisms underlying breast cancer resistance to RT is of paramount importance to overcome this clinical challenge.

While therapeutic resistance has been traditionally viewed with a cancer cell-centric bias, there is an increasing appreciation that the tumor microenvironment (TME) also plays an important role [5]. Cancer-associated fibroblasts (CAFs) are the most prevalent constituent cell type in the TME of many cancers, including breast, pancreas, and hepatic carcinomas [6, 7]. In human breast tumors, the abundance of stromal myofibroblasts (i.e., α-smooth muscle actin αSMA$^+$ fibroblasts) correlates with an aggressive phenotype and predicts disease recurrence [8] [9]. Indeed, a higher abundance of CAFs predicts resistance to drug and RT in many solid cancers, including rectal, lung and pancreatic cancers [10, 11]. However, it remains poorly understood whether CAF-driven radioresistance is relevant in the context of

breast cancer and, if so, how CAFs may be recruited and mechanistically contribute to this process.

Crosstalk between cancer cells and the TME involves reciprocal juxtacrine and/or paracrine signaling. Indeed, the Notch signaling pathway is recognized as a major factor in both cancer cells and components of the TME [12, 13]. The Notch pathway is composed of 4 receptors (Notch1–4) and 5 membrane-bound ligands (Jagged1, 2 and Dll1, 3 and 4), and its activity regulates differentiation, proliferation, angiogenesis, resistance and cell death through direct cell-to-cell signaling [13]. Although the Notch pathway is frequently deregulated and is one of the crucial contributors to cancer stem cell (CSC) self-renewal, invasion and infiltration of a variety of stromal cells in breast cancer [14], it remains unclear how these pathways may interact to promote radioresistance, recurrence, and metastasis in breast cancer.

We had previously shown that Dll1 overexpression correlates with poor prognosis in ERα$^+$ luminal breast cancer, but not in other subtypes of breast cancer [15]. Here, we demonstrate an increase in the expression of DLL1 in tumor cells and αSMA$^+$ and FAP$^+$ CAFs in ER$^+$/PR$^+$ breast cancer patients receiving RT and find that this phenotype is associated with more rapid recurrence and metastasis. METABRIC data analysis further reveals a strong correlation between *DLL1* and *FAP* as well as *ACTA2* (encoding αSMA) in ER$^+$/PR$^+$ luminal breast cancer post radiation, suggesting DLL1 along with CAF markers could be used to predict those patients with poor clinical outcome after radiation. ScRNA-seq and immunofluorescence data show a strong association between Dll1 and αSMA$^+$ myofibroblastic CAFs (myCAFs) and FAP$^+$ activated CAFs in luminal mouse breast tumors with high Dll1 levels. Using Dll1^{mCherry} reporter and Dll1 conditional-knockout (Dll1^{cKO}) mouse models carrying a MMTV-PyMT transgene to model aggressive luminal breast cancer, we further show that Dll1$^+$ CSCs recruit CAFs to the TME by producing IL-6. Genetic knockout or pharmacological blocking of Dll1 renders Dll1$^+$ tumor cells significantly more sensitive to radiotherapy. Combined targeting of Dll1 and IL-6 by antibodies also makes these tumors sensitive to radiation, opening new avenues of treatment in patients who will likely become radioresistant. Mechanistically, our studies with murine tumors and patient derived xenograft suggest that high Dll1 and increased CAF expression may serve as a biomarker for patients who will be non-responsive to RT and provides the basis for future combination therapy targeting Dll1-mediated Notch and Wnt signaling in tumor and CAFs to combat radioresistance.

Materials and methods

Human patient samples

De-identified breast cancer specimens used in the study were obtained from the Eastern Division of the Cooperative Human Tissue Network (CHTN), University of Pennsylvania. Details of all patient samples are listed in Supplementary Table S1. All samples were considered exempt by the Institutional Review Board of University of Pennsylvania. The H-Score was calculated by multiplying intensity with abundance. More details on animal studies are available in supplemental file.

Animal studies

All animal procedures were approved and conducted in compliance with the Institutional Animal Care and Use Committee (IACUC) of the University of Pennsylvania. MMTV-PyMT Dll1^{mCherry} (hereafter referred to as Py-Dll1^{mCh}) reporter mice and MMTV-PyMT-Dll1^{WT} (hereafter, referred to as Py-Dll1^{WT}) and MMTV-PyMT-Dll1^{cKO} (hereafter referred to as Py-Dll1^{cKO}) mice used in this study have been described previously [16]. Six-week-old female wild-type C57/BL6 for orthotopic MFP injection were obtained from Jackson Laboratory. For MFP injections, all mice were anesthetized, and tumor cells were injected into the MFP following the established protocol [15]. Contralateral mammary gland injection was performed in each mouse with the same number of tumor cells as mentioned in the corresponding figure legends. Tumors were detected by palpation and measured once a week. 6 Gy Targeted radiation (TRT) at a dose of 6 Gy using SARRP radiation machine was given to the implanted site of MFP when tumors achieved an established size (indicated in respective legends). For TRT, SARRP radiation machine was used. For whole body radiation (WRT) experiments, spontaneous Py-Dll1^{mCh} tumor-bearing mice were exposed to a 6 Gy dose in a gamma irradiator machine (MDS Nordion, USA). The experiment was terminated after 6 days (short-term) or 40–50 days (long-term) following TRT, and 6 days of WRT as mentioned in respective figure legends. Tumor size was assessed by external measurement of length (L) and width (W). The tumor volume (mm^3) was calculated by using the following equation: tumor volume = [(π L × W2)/6]. During the experiment, the animals were closely monitored for any signs of morbidity, declining body weight, ruffled fur, hunched posture, and ulceration of tumor. Anti-immunoglobulin G (IgG), anti-Dll1-blocking antibody (18 mg/kg) and anti-IL-6 antibody (20 mg/kg) antibodies were given on alternate days as mentioned in the respective figure legends. Tumors were palpated weekly. The experiment was terminated when tumors reached certain size as mentioned in the respective figure legends, or before if the tumors were ulcerated (humane endpoint).

Cell culture studies

Mouse WTB cell line was a kind gift from Dr. Yibin Kang's laboratory, Princeton University, NJ. And was confirmed to be mycoplasma negative by PCR (catalog no. ATCC, 30–1012K). WTB cell line was cultured and maintained in Dulbecco's Modified Eagle's Medium (DMEM) with high glucose (4.5 gm/ml) (Invitrogen, catalog no. 11965084). Primary tumor cell lines from Py-Dll1$^{WT/cKO}$ or Py-Dll1$^{mCh+/-}$ spontaneous tumors were maintained in Mammary Epithelial Cell Growth Medium (MEGM) (Invitrogen, catalog no. 11330032), supplemented with growth factors [15–17]. Patient derived xenograft (PDX) cells were cultured and maintained in Human Breast Epithelial Cell (HBEC) media supplemented with growth factors [18]. All cells were supplemented with 10% heat-inactivated fetal bovine serum (FBS) (Gemini, catalog no. 900108) and 100 U/ml penicillin and 100 μg/ml streptomycin sulfate (Invitrogen, catalog no. 15140122).

For co-culture assays, drugs used are as follows: DLL1 antibody (200 ng/ml) [16], DAPT (Gamma secretase inhibitor-GSI) (200 ng/ml) (Sigma-Aldrich, catalog no. D5942–5MG), JW74, a canonical Wnt signaling inhibitor (10μM) (Tocris bioscience, catalog no. 5653) and LGK-974, a porcupine inhibitor that inhibits secretion of Wnt ligands (10μM) (Selleckchem, catalog no. CS7143).

Co-culture and tumorsphere assay

Briefly, single cells from Py-Dll1$^{WT/cKO}$ primary tumors and PDX tumors were made following the published protocol [18, 19]. We sorted mouse CAFs from Py-Dll1^{WT} tumor based on F4/80 and CD140a (PDGFRα) antibodies and human CAFs were sorted from ER^{+}/PR^{+} fresh human tumor tissues based on EPCAM and CD140a (PDGFRα) antibodies respectively. TAMs were sorted from Py-Dll1^{WT} tumors based on CD45 and F4/80 antibodies. Details of all antibodies are listed in the Supplemental Table S3. For the co-culture and tumorsphere assays, both the primary tumor cells and Dll1 overexpressing (Dll1-OE) WTB cells were co-cultured with CAFs or TAMs as previously described protocol [20]. Briefly, a total number of 20,000 tumor cells and 4,000 of either CAFs or TAMs were successfully cultured in Corning low adherent plates in serum-free tumorsphere cell suspension media for 3 days as tumorspheres following established protocol [15]. Tumorspheres were given ionizing radiation at room temperature with an acute dose of 6 Gy after 48–72 hours of plating. Following radiation, co-cultured cells were further cultured for 72 hours, during which time spheres were imaged and quantified for 24, 48 and 72 hours (Fig. 6B–D; Supplementary Figs. S11A–S11D) using a Nikon TiE microscope. In addition, following 6 hours of radiation, spheres were treated with DLL1 antibody (200 ng/ml) [16], DAPT (Gamma secretase inhibitor-GSI) (200 ng/ml) (Sigma-Aldrich, catalog no. D5942–5MG), JW74, a canonical Wnt signaling inhibitor (10μM) (Tocris bioscience, catalog no. 5653) and LGK-974, a porcupine inhibitor that inhibits secretion of Wnt ligands (10μM) (Selleckchem, catalog no. CS7143) in different experiments as indicated in the corresponding figure legends and were further cultured for 72 hours. The number of spheres were imaged and quantified at 72 hours under a Nikon TiE light microscope per filed of view (FOV).

Statistics and reproducibility

We repeated our *in vitro* experiments at least two times in duplicate. We used a minimum of 3 mice per group for *in vivo* experiments, exception in Supplementary Fig. S7N, where one mouse was dead before completion of experiment. For *in vivo* experiments, the mice were randomized based on their age and body weight, before the start of the experiment. The results are reported as mean ± SEM (standard error of the mean). The significance of differences was calculated using two-tailed unpaired student *t*-test for normally distributed datasets. Paired two-tailed student *t*-test was done to compare matched primary and recurrent breast tumors (Supplementary Fig. S7C–S7H). One-way ANOVA with TUKEY's multiple comparisons post hoc test was used for multiple comparisons. The tumor growth and grouped datasets were analyzed using the Bonferroni corrected two-way ANOVA to compute statistical significance. GraphPad Prism 8 software was used for all statistical analyses. The number of animals and the statistical tests to compute p-value are reported in each of the corresponding figure legends.

Additional methods are in supplemental file.

Data availability

The data generated in this study are available within the article and its Supplementary Data file. Bulk RNA-seq data is available in GSE172399 and GSE172398. Sc-RNA-seq data is available in GSE182011.

Results

Increased DLL1$^+$ tumor cells and FAP$^+$ and αSMA$^+$ CAFs in breast cancer patients who have undergone radiotherapy

We had previously shown that DLL1 expression correlates with poor prognosis in ERα$^+$ luminal breast cancer, but not in other subtypes of breast cancer [15]. To determine if DLL1 mediated Notch signaling also impacts human breast cancer post-radiation, we performed immunohistochemistry (IHC) on three independent cohorts of tumor samples from ER$^+$/PR$^+$ luminal patients (non-TNBC) who did not receive radiation or were undergoing RT in an adjuvant (ART) or neoadjuvant (NART) setting (Supplementary Table S1). H-score data on luminal breast tumor samples indicated higher expression of DLL1 protein in NART tumors when compared to RT breast tumors (p=0.01) or ART patients' tumors (p=0.60) (Fig. 1A and B), suggesting radiation induces DLL1 expression or increases the number of DLL1$^+$ cells in the NART setting. Higher DLL1 levels were not observed in ART tumors and no conclusions can be drawn potentially due to low sample size. Moreover, cytokeratin 14 (K14), a stem/basal progenitor marker that is associated with poor prognosis and decreased relapse-free and overall survival [21], was expressed higher in luminal tumors after NART relative to tumors without radiation (p=0.04), but a similar increase was not observed in tumors from the ART setting (p=0.58) (Fig. 1C and D). Consistent with our published data and recent emerging studies that highlight the pleiotropic roles of cancer associated fibroblasts (CAFs) in mammary gland development [20], cancer progression and acquisition of therapeutic resistances [6], our immunofluorescence (IF) data indicates that NART and ART luminal tumors have a greater abundance of α smooth muscle actin positive (αSMA$^+$) CAFs (p=0.03 and 0.0002) compared to -RT (Fig. 1E and F). Similarly, NART luminal tumors have a higher number of fibroblast activated protein positive (FAP$^+$) activated CAFs than -RT luminal patient tumors (p=0.03). There was no increase in activated CAFs in the small number of ART tumors analyzed compared to -RT (p=0.70) (Fig. 1G and H). Together, these data suggest that high CAF abundance and increased numbers of DLL1$^+$ tumor cells correlate with poor patient outcome post irradiation in a NART setting. Interestingly, from a large cohort of METABRIC dataset patients who received radiation, we found a strong positive correlation between mRNA levels of *DLL1* to *FAP* (r= 0.29, p<0.0001) and *ACTA2* (r= 0.47, p<0.0001) after radiation in luminal breast cancer patients (n= 563) (Fig. 1I and J). Unlike the strong correlation of DLL1$^+$ cells and FAP$^+$ cells in luminal tumors post radiation, there were no significant alterations in CD163$^+$ tumor associated macrophage (TAM) population in these patient samples post NART compared to tumors without RT (p=0.84) (Supplementary Fig. S1A and S1B).

In addition, ER$^+$/PR$^+$ luminal breast cancer showed no significant changes were observed in either DLL1 expression (p=0.39) or αSMA$^+$ (p=0.78) or FAP$^+$ CAFs (p=0.48) post NART/ART compared to -RT ER$^-$/PR$^-$/HER2$^-$ (TNBC) patient tumors (Supplementary

Fig. S1C–S1H), suggesting that the correlation between DLL1 and FAP is highly specific to ER^+/PR^+ luminal tumors. Interestingly, K14 expression (p=0.009) was significantly increased in TNBC tumors that had undergone NART (Supplementary Fig. S1I and S1J). IHC analysis of TNBC patient's tumor sections showed no significant changes in DLL1, αSMA, FAP or K14 expression in TNBC tumors before and after ART (Supplementary Fig. S1C–S1J), which could be due to low sample size. Together, our data show that ER^+/PR^+ patients with poor clinical outcome post radiation is specifically associated with a higher abundance of $DLL1^+$ tumor cells and CAFs, suggesting DLL1 may have causal role in driving CAF-mediated radioresistance of non-TNBC or luminal tumors.

Single cell transcriptome profiling reveals increased myCAFs and FAP^+ activated CAFs in $Dll1^+$ but not in $Dll1^-$ tumors

CAFs coexist as heterogeneous populations with potentially different biological functions [22]. To survey the diverse fibroblast populations of aggressive luminal breast cancer (non-TNBC) at a cellular level, we utilized a recently published MMTV-PyMT-$Dll1^{mCherry}$ (hereafter referred to as Py-$Dll1^{mCh}$) reporter breast cancer mouse model [16, 20] generated by mating $Dll1^{mCherry}$ reporter mice with luminal MMTV-PyMT mice [16]. Seurat based 10x scRNA-seq analyses from $Dll1^+$ and $Dll1^-$ tumors (Fig. 2A) showed 14 clusters of $CD45^-$ cells and notably, *Dll1* was higher in cluster 1, 3 and 5 (Fig. 2B–D). Based on *keratin* (*Krt8*, *Krt18* and *Krt14), and Epcam* expression, clusters 0–3, 5–8 and 11–12 were defined as epithelial cell clusters (Supplementary Fig. S2A). Moreover, clusters 4 and 10 were enriched for CAF populations based on standard CAF markers [22] (Fig. 2E and F; Supplementary Fig. S2B). Recently, *Bartoschek et al.*, and *Sebastian et al.*, [7, 22] identified six distinct CAF populations including $Acta2^{high}$ myofibroblastic CAFs (myCAFs), vascular regulator enriched $Notch3^{high}$ CAFs (vCAFs), and $Ly6c^{high}$ inflammatory CAFs (iCAFs). Based on differential gene expression [22], we found that cluster 10, which is higher in $Dll1^+$ tumors, likely consists of vCAFs and myCAFs (Fig. 2C and F; Supplementary Fig. S2C). Consistent with this finding, IF and IHC analyses revealed an increase in FAP^+ and αSMA^+ CAFs in $Dll1^+$ tumors compared to $Dll1^-$ tumors (Fig. 2G–J). On the other hand, cluster 4, which contains iCAFs, was enriched in $Dll1^-$ tumors relative to $Dll1^+$ tumors (Fig. 2C and F; Supplementary Fig. S2C). We also found that cluster 4 CAFs are enriched in genes from $CD53^{high}$ CAFs and genes for $Crabp1^{high}$ CAFs (Supplementary Fig. S2C). Notably, higher expression of *Notch2* and Notch signaling target genes such as *Hes1* and *HeyL* was observed in cluster 10 CAF populations (Supplementary Fig. S2D), which were higher in $Dll1^+$ tumors. Taken together, these results suggest that increased abundance of myCAFs is strongly associated with high Dll1 levels and that Notch target genes are upregulated in different CAF subtypes at baseline in luminal breast tumors.

To further confirm the correlation between CAFs and Dll1, we employed a syngeneic breast cancer mouse model using a Dll1-overexpressing (OE) WTB luminal breast cancer cell line derived from a MMTV-PyMT transgenic mouse tumor [15]. IF and IHC analyses with control WTB ($Dll1^{low}$) and Dll1-OE WTB ($Dll1^{high}$) xenograft tumors showed a significant increase in the abundance of CAFs (αSMA^+ and FAP^+) in Dll1-OE WTB tumors relative to control tumors (Fig. 2K–N), suggesting that $Dll1^+$ tumor cells may recruit unique CAF subsets (αSMA^+ and FAP^+ CAFs) to these aggressive luminal tumors.

Increased numbers of Dll1$^+$ CSCs are associated with increased metastases, high FAP$^+$/αSMA$^+$ CAF infiltration and hypoxia in Dll1$^+$ primary breast tumors post radiation

To determine the importance of the radiation-induced increase in Dll1$^+$ cells in tumor progression and metastasis (Supplementary Fig. S3A–S3E), we used the established Py-Dll1^{mCh} mouse model [16]. Following 12 Gy of WRT, significant loss of body weight was observed in irradiated mice compared to control mice whereas 6 Gy treated mice showed no significant weight loss (Supplementary Fig. S3B and S3D), further experiments used only a single dose of 6 Gy radiation. In this scenario, reductions in tumor size were not observed due to the short response window of 6 days (Supplementary Fig. S3C and S3E).

Based on clinical studies, targeted radiation (TRT) of the primary tumor appears adequate for achieving local control of cancer [23]. Therefore, we tested the efficacy of TRT on transplanted Dll1$^+$ and Dll1$^-$ tumor cells derived from Py-Dll1^{mCh} reporter mice into the mammary fat pad (MFP) of syngeneic C57BL/6 mice (Supplementary Fig. S3F). Notably, neither short nor long-term 6 Gy TRT treatment resulted in significant weight loss (Supplementary Fig. S4A and S4B). Notably, long-term TRT treatment was unable to prevent Dll1$^+$ tumor progression, but significantly reduced tumor growth and progression of Dll1$^-$ tumors (Fig. 3A–D), suggesting that Dll1$^+$ tumor cells *in vivo* are radioresistant.

To determine if there was an association between Dll1 mediated radioresistance and metastasis, we assessed tumor burden in the lung and bones, two traditional sites of metastasis in patients who do not respond to RT [24, 25]. Interestingly, we found a greater number of metastatic nodules after TRT in the lungs of Dll1$^+$ tumor bearing mice compared to no radiation mice (Fig. 3E–G). We also found more metastatic nodules in TRT Dll1$^+$ tumor bearing mice compared to TRT Dll1$^-$ tumor bearing mice (Supplementary Fig. S4C and S4D), suggesting Dll1-dependent radioresistance is associated with metastasis. Furthermore, we observed more Dll1^{mCh+} cells in the bone of Dll1$^+$ tumor cell bearing mice post TRT (Supplementary Fig. S4E and S4F). The bone marrow is a preferred metastatic site for disseminated tumor cells (DTCs) in several solid tumors, such as breast cancer, lung cancer, prostate cancer and others [26] and correlates with disease recurrence in many cancer types including breast cancer [27, 28]. To determine if Dll1^{mCh+} tumor cells accumulate in the bone marrow of recipient C57BL/6 mice following orthotopic transplantation of Dll1$^+$ tumor cells, we extracted bone marrow cells and cultured them *ex vivo*. Bone marrow from irradiated Dll1$^+$ tumor bearing mice demonstrated a significant increase in the number of Dll1$^+$ tumor cells (based on mCherry) (Supplementary Fig. S4G and S4H), similar to our *in vivo* data. In addition, the number of Dll1^{mCh+} tumor cells in the blood were significantly higher in Dll1$^+$ tumor cell bearing mice after long-term TRT compared to the untreated mice (Supplementary Fig. S4I and S4J), suggesting that radioresistant Dll1$^+$ tumor cells may represent DTCs, capable of seeding distant organ metastasis. Collectively, our results suggest that Dll1$^+$ tumor cells but not Dll1$^-$ tumor cells are a critical determinant of radioresistance, associated with dissemination of tumor cells followed by distant organ metastasis.

Cancer stem cells (CSCs) are thought to be responsible for radioresistance in various cancers [29]. Notably, we observed a significant increase in the CSC (CD24$^-$CD44^{high}) population [30] in Dll1$^+$ tumors post long-term TRT, while dramatic reduction in the CSC

(CD24^{-}CD44^{+}) population in TRT Dll1^{-} tumors compared to non-irradiated Dll1^{-} tumors (Fig. 3H). Notably, a significant increase in the number of Dll1^{mCh+} cells was found in Dll1^{+} tumors post long-term TRT (Fig. 3I). Our recent published report indicates that Dll1^{+} tumor cells bear a stem cell like phenotype [16]. Therefore, we next investigated if Dll1$^{mCherry+}$ stem-like cells are part of the established CD24^{-}CD44^{+} CSC population [30] in these tumors. Flow cytometry analysis (FACS) revealed a significant overlap of Dll1^{mCh+} cells with CD24^{-}CD44^{+} CSCs, which were significantly more abundant in TRT irradiated Dll1^{+} tumors (Fig. 3J) compared to untreated tumors, which further suggests that the radioresistance of Dll1^{+} tumor cells is associated with an increase in the number of Dll1^{mCh+} CSCs (Dll1^{+}CD24^{-}CD44^{+}).

Next, we determined if the increase in Dll1^{+}CSCs, DTCs, and metastases correlates with an increase in the number of CAFs within the TME post radiation. FACS analysis revealed an increase in the total number of CD140^{+} CAFs (CD45^{-}CD140^{+}) in TRT treated Dll1^{+} tumors (Fig. 3K). In addition, using standard CAF markers such as αSMA, CD140/PDGFR-α, CD90 (Thy1) and FAP [22, 31], we found that αSMA^{+} CAFs increase significantly in primary Dll1^{+} tumors after long-term TRT. Moreover, higher number of Dll1^{mCh+} tumor cells was further confirmed by IF in primary TRT- Dll1^{+} tumors compared to untreated Dll1^{+} tumors (Fig. 3L–3N). Notably, increase number of FAP^{+} CAFs were observed in TRT treated Dll1^{+} tumors (Fig. 3O and P). FACS further confirmed that FAP^{+} CAFs (CD45^{-}CD90^{+}FAP^{+}) and αSMA^{+} myCAFs (CD45^{-}FAP^{+}αSMA^{+}) increase significantly in primary Dll1^{+} tumors after long-term TRT (Fig. 3 Q and R), corroborating our scRNA-seq data (Fig. 2F). Consistent with long-term TRT, similar results were observed after short-term TRT (Supplementary Fig. S5A–5D) and 6 days post-WRT (Supplementary Fig. S5E–S5H), suggesting that the increase in number of CAFs occurs early post radiation. Notably, we observed a decrease in αSMA^{+} myCAFs in long-term TRT Dll1^{-} primary tumors (Supplementary Fig. S5I and S5J). Taken together, these findings suggest that the Dll1-dependent increase in the total CAF subpopulation that occurs post-irradiation may play a critical role in breast cancer radioresistance and metastasis. This was further confirmed by clonogenic assays with Dll1^{+} or Dll1^{-} tumor cells with CAF conditioned media showing a significant decrease in the survival fraction of the Dll1^{-} tumor cells after radiation compared to Dll1^{+} tumors cells (Supplementary Fig. S5K), further supporting the radioresistant phenotype of Dll1^{+} tumors cells and radiosensitive phenotype of Dll1^{-} tumor cells.

Intratumoral hypoxia and increased production of reactive oxygen species (ROS) are considered hallmarks of cancer and are associated with chemo/radioresistance, as well as disease progression and evolution toward metastatic phenotypes [32]. IF showed an increased abundance of CAIX^{+} cells in TRT treated Dll1^{+} primary tumors relative to untreated tumors. In addition, the number of double positive CAIX^{+} Dll1^{mCh+} cells were significantly higher in irradiated Dll1^{+} breast tumors (Supplementary Fig. S5L and S5M). No difference in CAIX^{+} cells were observed in TRT treated Dll1^{-} tumors compared to untreated tumors (Supplementary Fig. S5N and S5O). Finally, we found a significantly higher number of single K14^{+} cells and double positive Dll1^{mCh+} K14^{+} tumor cells in TRT irradiated Dll1^{+} primary tumors (Supplementary Fig. S5P and S5Q) compared to untreated tumors, supporting our human data (Fig. 1C and D). Consistent with the findings from

long-term TRT, similar findings were observed 6 day post TRT and WRT (Supplementary Fig. S6A–S6H), suggesting Dll1^{+} tumor cells rapidly become hypoxic and more basal/stem like post radiation. Collectively, our data strongly supports a strong positive association between radioresistance and increased numbers of hypoxic Dll1^{+} tumor cells with a stem cell like phenotype.

Pharmacological inhibition of Dll1 in recurrent tumors abrogates tumor growth, metastases and CAF infiltration

We next asked if the Dll1 associated phenotypes in primary tumors were also apparent in recurrent tumors that arose from primary tumors removed after RT (6 Gy of TRT was given), thus mimicking NART (Supplementary Fig. S7A). Tumors were resected when they were ~100–150 mm^3 in size. Dll1^{+} tumors that recurred following TRT and resection grew rapidly. Interestingly, IF analyses reveal a significant increase in the number of Dll1^{+} tumor cells and αSMA^{+} myCAFs in the recurred (Recur) tumors when matched with primary resected tumor (Pri) (Supplementary Fig. S7B–S7D), suggesting a causal role for Dll1 in driving recurrence post RT. Flow cytometric analyses further revealed that recurrent Dll1^{+} tumors showed a greater number of Dll1^{+} cells, α-SMA^{+} myCAFs and CD140^{+} CAFs (Supplementary Fig. S7E–S7G) compared to their matched primary tumors. A further modest increase in CSCs (CD24^{-}CD44^{+}) were seen in recurrent Dll1^{+} tumors compared to their primary tumors (p=0.08) (Supplementary Fig. S7H), suggesting a Dll1^{+}CSC dependent radioresistant phenotype of recurred tumors.

Next, we investigated whether pharmacological blocking of Dll1 *in vivo* could reduce recurrence post radiation. For this, mice bearing primary Dll1^{+} tumors followed by orthotopic injection of tumor cells, were subjected to TRT, and tumors were subsequently resected. Following resection, tumor bearing mice were given either isotype IgG control or anti-Dll1-blocking antibody and recurred tumors were measured over time. Pharmacological blocking of Dll1 activity significantly decreased tumor progression and lung metastasis (Supplementary Fig. S7I–S7M). Moreover, the number of Dll1^{mCh+} cells was significantly decreased in bone marrow (BM) and blood upon Dll1 blocking as demonstrated by Flow cytometry (Supplementary Fig. S7N and S7O). This finding suggests that blocking Dll1 can decrease Dll1-dependent recurrence in a NART setting. Following pharmacological inhibition of Dll1, we also observed a significant reduction of CD140^{+}, αSMA^{+} myCAFs and CD45^{-}FAP^{+}CD90^{+} CAFs (Supplementary Fig. S7P–S7S) in Dll1^{+} recurred tumors, which further supports that Dll1 mediated radioresistance and recurrence are potentially driven by recruitment/abundance of CAFs in the TME of irradiated luminal breast tumors.

Conditional knockout of Dll1 decreases tumor progression, lung metastasis and abundance of αSMA^{+} myCAFs in luminal tumors post radiation

To determine if Dll1 is crucial for tumor progression and lung metastasis upon TRT, sorted Dll1^{WT} and Dll1^{cKO} tumor cells from spontaneous MMTV-PyMT; Dll1^{WT} (hereafter referred to as Py-Dll1^{WT}) and MMTV-PyMT; Dll1^{cKO} (hereafter referred to as Py-Dll1^{cKO}) tumor-bearing mice that we recently generated [16, 20] were orthotopically implanted into recipient C57BL/6 immunocompetent mice and subjected to a single 6 Gy dose of TRT when tumors were established at 2–3 weeks post injection. TRT- Dll1^{WT} (+TRT) tumors

both progressed and developed metastatic nodules in the lungs more quickly than did non-irradiated (-RT) Dll1^{WT} tumors (Fig. 4A–C). In contrast, TRT- Dll1^{cKO} (+TRT) tumors progressed more slowly than non-irradiated (-RT) Dll1^{cKO} tumors (Fig. 4D and E). The low level of lung metastasis post radiation was not significantly different between the Dll1^{cKO} tumor bearing mice groups (Fig. 4F), further supporting a causative role for Dll1 in the radioresistant phenotype associated with increased metastasis. Interestingly, there was a dramatic increase in the CD24^{-}CD44^{+} CSC population in Py-Dll1^{WT} tumors post radiation (long term) (Fig. 4G). Similar to the Py-Dll1^{mCh} reporter model, we found that conditional knockout of Dll1 in tumor cells (Py-Dll1^{cKO}) led to a dramatic reduction in the surviving fraction compared to Dll1^{WT} tumor cells after radiation with CAF CM in the clonogenic assay (Supplementary Fig. S8A), further indicating that Dll1^{+}/Dll1^{high} tumor cells are radioresistant.

Similar to genetic conditional knockout of Dll1 (Dll1^{cKO}), pharmacological blocking of Dll1 also sensitized radioresistant Dll1 high (Dll1^{WT}) tumor cells to radiation, as seen by decreased tumor progression, lung metastasis and CSC population (Fig. 4H–K), suggesting that Dll1-dependent CSC function is associated with radioresistance and metastasis in luminal breast cancer. Consistent with our findings from the Dll1^{mCh+} reporter mouse model, we found a significant increase in CAIX^{+} cells and K14^{+} cells (Supplementary Fig. S8B–S8E) in +TRT Py-Dll1^{WT} tumors compared to -RT Py-Dll1^{WT}. Fewer CAIX^{+} cells and K14^{+} cells were observed in irradiated Py-Dll1^{cKO} tumors compared to non-irradiated Py-Dll1^{cKO} tumors (Supplementary Fig. S8F–S8I). In addition, we found a significant decrease in CAIX^{+} cells (Supplementary Fig. S8F and S8G) and modest decrease in K14^{+} cells (Supplementary Fig. S8H and S8I) in +TRT Py-Dll1^{cKO} tumors compared to -RT Py-Dll1^{cKO} tumors. Notably, there were significantly more αSMA^{+} and FAP^{+} CAFs in +TRT Py-Dll1^{WT} tumors compared to untreated Py-Dll1^{WT} tumors (Fig. 4L–O). In addition, decreased number of αSMA^{+} CAFs in +TRT Py-Dll1^{cKO} tumors compared to non-irradiated Py-Dll1^{cKO} tumors (Fig. 4P and Q). Similar to genetic conditional knockout of Dll1, pharmacological blocking of Dll1 in Py-Dll1^{WT} tumors reduced the number of αSMA^{+} and FAP^{+} CAFs (Fig. 4R–T and Supplementary Fig. S8J). Taken together, these findings suggest genetic or pharmacological blocking of Dll1 activity sensitizes tumors to radiation and also reduces the radiation associated hypoxic phenotype, as well as the number of K14 expressing basal/stem like tumor cells and αSMA^{+} and FAP^{+} CAF populations in TME.

Secreted IL-6 from Dll1^{high} tumor cells potentiates recruitment of myCAFs to the breast TME post radiation and can be reverted by pharmacological blocking of IL-6/Dll1 signaling

Stromal cell migration and invasion are considered critical for acquired therapeutic resistance and are regulated by numerous tumor-secreted factors among which IL-6, IL-12, Cxcl-12 and Tgf-β1 play pivotal roles by altering the TME to promote therapeutic resistance in many solid cancers [33–36]. To determine if the increased numbers of CAFs present in our radioresistant luminal breast cancer experimental model could be linked to enhanced recruitment in response to a tumor cell secreted factor, we performed quantitative RT PCR (qPCR) analyses which revealed that the mRNA expression of *IL-6, IL-12,* and *Cxcl-12* are consistently up-regulated in irradiated Dll1^{+} tumor cells compared to control -RT Dll1^{+} tumor cells (Supplementary Fig. S9A and S9B), suggesting that radioresistant Dll1^{+} tumor

cells may drive CAF recruitment. Complementary to this approach, unbiased bulk mRNA sequence analysis showed that a total number of 221 genes were significantly upregulated in sorted Dll1^{+} tumor cells after radiation, whereas only 35 genes were downregulated in sorted Dll1^{+} tumor cells with no radiation (Fig. 5A), thereby identifying a distinct radiation-induced gene expression profile in Dll1^{+} cells. Interestingly, we found that the IL-6/JAK-STAT3 pathway is significantly upregulated in Dll1^{+} tumors post radiation (Fig. 5B), supporting earlier data indicating dramatic increased *IL-6* mRNA expression in tumor cells post radiation (Supplementary Fig. S9A and S9B). This observation was further confirmed by IL-6 protein data using FACS analysis and ELISA (Fig. 5C and D). Furthermore, western blot analysis revealed that activation of the STAT-3 signaling pathway (enhanced p-STAT-3, downstream of IL-6 signaling) occurs in CAFs sorted from Dll1^{+} tumors after radiation (Fig. 5E), suggesting that IL-6 produced by Dll1^{+} tumor cells is responsible, at least in part, for activating CAFs within the TME.

Next, transwell migration assay revealed that CM from Py-Dll1^{WT} primary tumor cells promoted greater CAF migration, which was reversed by blocking IL-6 using anti IL-6 antibody (Fig. 5F). Addition of IL-6 recombinant protein to plain media also showed increased migration of CAFs, further supporting the requirement of IL-6 specifically in CAF migration. In complementary gain-of function studies, CM from Dll1-OE WTB luminal cells (derived from MMTV-PyMT) recruits more CAFs compared to CM from control WTB cells (Dll1^{low}) (Supplementary Fig. S9C). This increase in CAF migration was prevented by addition of anti-IL-6 blocking antibody, suggesting that IL-6 is a central mediator of CAF migration downstream of Dll1 in luminal breast cancer.

IL-6 induction is associated with a poorer prognosis in patients with metastatic breast cancer and serum IL-6 levels are associated with an increase in pathological tumor grade [37]. Although blocking of IL-6 signaling with monoclonal antibodies specific for IL-6 has proven its worth in many preclinical studies, the response to anti-IL-6 monotherapy in breast cancer post radiation is limited [38, 39]. Therefore, we next determined if blocking of IL-6 signaling coupled with blocking of Dll1 using anti-Dll1-blocking antibodies could further sensitize the tumors to TRT following orthotropic injection of Py-Dll1^{+} tumors cells from Py-Dll1^{mCh} mouse model in C57BL/6 recipient mice (Fig. 5G). Radiation followed by drug treatment was started when tumors were at an early stage (6mm×6mm) to allow further CAF recruitment with tumor progression. Tumor progression and lung metastasis were significantly reduced post combination therapy as well as after monotherapy with either anti-Dll1 or anti-IL-6 antibody (Fig. 5H–K), suggesting Dll1-dependent CAF recruitment is an important step in driving resistance to radiation. The decrease in tumor growth and lung metastases in the drug treatment cohort of mice was associated with reduced abundance of CSC (Fig. 5L), Dll1^{+} and Dll1^{+} CSCs (Supplementary Fig. S9D and S9E) and αSMA^{+} myCAF and FAP^{+} activated CAF and also CD140^{+} and FAP^{+}CD90^{+} CAF populations in primary Dll1^{+} tumors (Fig. 5M–O; Supplementary Fig. S9F and S9G), suggesting that Dll1^{+} CSCs drive metastasis through CAF recruitment.

Finally, Gene Set Enrichment Analysis (GSEA) identified several radio-resistant signatures, including ROS, angiogenesis and epithelial-to-mesenchymal transition (EMT) pathways [40] that were enriched in sorted Dll1^{+} cells from irradiated tumors (Supplementary Fig. S9H–

S9J). Intracellular ROS levels were also determined by DCF-DA assay, which revealed a greater level of intracellular ROS production in TRT irradiated Dll1^{+} tumor cells compared to non-irradiated Dll1^{+} tumors (Supplementary Fig. S9K), corroborating our bulk mRNA sequencing data. Furthermore, the intracellular ROS-dependent radioresistant phenotype of Dll1^{+} tumor cells were prevented by exogenous addition of catalase (25 units/ml) in co-culture with sorted CAFs (Supplementary Fig. S9L), which further suggest that ROS plays an important role in maintaining the radioresistant function of Dll1 through CAFs. In addition, upregulation of several radiation pathways was observed in irradiated Dll1^{+} tumor cells compared to untreated Dll1^{+} tumor cells (Supplementary Table S2A).

CAFs recruited in the TME post radiation augment stemness of Dll1^{+} tumor cells through activation of Wnt signaling

Recent studies revealed that Notch activation in CAFs is associated with disease progression, however its role in conferring radioresistance in breast cancer remains unclear. Thus, we next assessed Dll1-activated Notch signaling in CAFs sorted from irradiated Dll1^{+} breast tumors based on CD140 (PDGFRα) antibody [20]. Quantitative PCR data revealed that sorted PDGFRα^{+} CAFs from post 40day irradiated Dll1^{+} mouse breast tumors express high levels of *Fap* and elevated levels of *Notch2* and *Notch3*, *bona fide* receptors for Dll1 ligand as well as Notch target genes *Hes2* and *HeyL* (Supplementary Fig. S10A–S10E). Consistent with our TRT data, similar trends in expression were observed from 6-day post WRT (Supplementary Fig. S10F–S10I). Overall, these results strongly suggest that activation of the Notch signaling pathway in CAFs by Dll1^{high} tumors after irradiation in aggressive luminal tumors involve Dll1-Notch2/3 interactions. Furthermore, bulk mRNA-seq analysis indicated that Wnt ligands were highly upregulated in sorted PDGFRα^{+} CAFs post radiation (Supplementary Table S2B). Like normal stem cells, the maintenance of CSC properties requires a supportive niche. While a recent clinical study supports the capacity of CAFs to promote the stemness of cancer cells [41], it is crucial to determine if and how they contribute to the acquisition of radioresistance in breast cancer. To this end, CAFs sorted from Py-Dll1^{WT} mouse tumors were co-cultured with primary tumor cells (enriched for tumor cells by sorting with Ter119, CD45 and CD31 antibodies) [17] derived from Py-Dll1^{WT} or Py-Dll1^{cKO} mouse tumors (Fig. 6A). Co-culture of Py-Dll1^{WT} tumor cells (with high Dll1 levels) with CAFs showed a greater number of tumorspheres compared to Py-Dll1^{cKO} cells in -RT context (Supplementary Fig. S11A). Additionally, we noted that co-culture of Py-Dll1^{WT} tumor cells with CAFs generated a greater number of tumorspheres post radiation compared to tumor cells alone suggesting that CAFs increase tumor cell stemness of Dll1^{WT} tumor cells (Fig. 6B and C). The tumor promoting effect of CAFs was not observed when Py-Dll1^{cKO} tumor cells (with low Dll1 levels) were used in co-culture, suggesting that Dll1 is necessary for the crosstalk between tumor cells and CAFs (Fig. 6B and C). As our earlier published work demonstrated that Dll1^{+} mammary epithelial cells can crosstalk with macrophages to promote stem cell function in normal breast [20], we performed similar *in vitro* tumorsphere assay of Py-Dll1^{WT} with Py-Dll1$^{WT/cKO}$ TAMs (tumor associated macrophages) post radiation (Supplementary Fig. S11B). Notably, addition of Py-Dll1^{WT} TAMs to Py-Dll1^{WT} tumor cells is associated with decrease in the number of tumorspheres post radiation, suggesting that TAMs do not contribute to the radioresistance of Dll1^{+} tumor cells (Supplementary Fig. S11C), corroborating human data.

To complement our loss-of-function study, we performed a similar co-culture assay with control and Dll1-OE WTB luminal breast cancer cells with Py-Dll1^{WT} CAFs (Fig. 6A). When cultured with Py-Dll1^{WT} CAFs, Dll1-OE WTB tumor cells formed significantly more tumorspheres compared to analogous cultures of control WTB tumor cells post radiation (Fig. 6D; Supplementary Fig. S11D). Taken together, our data strongly suggests CAFs promote Dll1 dependent CSC function post radiation.

Wnt signaling is known to function in breast cancer, particularly in TNBC [18, 42], but the function of Wnt signaling on hormone responsive breast cancer has not yet been explored in detail. Our unbiased bulk mRNA seq data strongly indicates that following radiation, Wnt ligand secretion by CAFs may promote Wnt signaling in tumor cells to further potentiate their stemness and promote radioresistance. Quantitative PCR data further confirmed that CAF educated radioresistant Py-Dll1^{WT} cells from co-culture express significantly higher Wnt target genes such as *Ccnd1 and Axin2* than do Py-Dll1^{WT} tumor cells alone (Fig. 6E). In further support, increased nuclear translocation of β-catenin in Py-Dll1^{WT} tumor cells following their co-culture with CAFs (Fig. 6F) post radiation, indicates activated Wnt signaling [43]. Notably, treatment with the Wnt inhibitor JW-74 [44], DAPT, a Notch inhibitor and anti-Dll1 antibody reverses β-catenin nuclear translocation and elicited a robust decrease in the number of tumorspheres in suspension co-cultures of CAFs and tumor cells post radiation further supporting a critical role for Wnt signaling in radioresistance (Fig. 6F–H), suggesting that Dll1 mediated Notch signaling is important for Dll1-Notch-Wnt crosstalk of tumor cells and CAFs post radiation.

To specifically evaluate the effect of Wnt secretion by CAFs, we used LGK-974, a porcupine inhibitor that specifically affects secretion of Wnt ligands [45] to prevent Wnt signaling and which is currently being evaluated in a clinical trial for Wnt-dependent malignancies (ClinicalTrials.gov Identifier: NCT01351103). LGK-974 reduced the number of tumorspheres and expression of Wnt target genes from Py-Dll1^{WT} tumor cells following their co-culture with CAFs post radiation when compared to irradiated Py-Dll1^{WT} tumor cells co-cultured with CAFs (Fig. 6I and J; Supplementary Fig. S11E). Finally, co-culture of CAFs with stable Py-Dll1^{WT}-7TGC tumor cells (lentiviral based Wnt-reporter plasmid, 7TGC [46]) (Supplementary Fig. S11F) showed significant activation of Wnt signaling (mCherry^{+}/GFP^{+} cells) as compared to Py-Dll1^{cKO}-7TGC tumor cells alone post radiation (Fig. 6K), confirming activation of Dll1-dependent Wnt signaling after radiation. To further determine if CAF affects activation of the Wnt/β-catenin pathway in a Notch receptor dependent manner, we made stable knockdowns of both Notch2 and Notch3 in Py-Dll1^{WT} CAFs using lentivirus, which was confirmed by qPCR (Fig. 6L; Supplemental Fig. S11G and S11H). Knockdown (KD) of either Notch2 or Notch3 in CAFs significantly reduced the number of tumorspheres and reduced nuclear localization of β-catenin in Py-Dll1^{WT} tumor cells following their co-culture with Notch2/3 KD1/KD2 CAFs post radiation (Fig. 6M–O; Supplementary Fig. S11I–S11K). Taken together, these findings clearly suggest that Notch2/3 expressing CAFs are most likely responsible for augmenting Notch-Wnt-dependent crosstalk with Dll1^{+} tumor cells, thereby promoting increases in stemness that can facilitate radioresistance.

Targeting DLL1 inhibits crosstalk with CAFs in DLL1^{high} patient derived xenograft (PDX) cells post radiation

To investigate whether our experimental findings could be relevant to the pathogenesis in human breast cancer, we next determined if the molecular crosstalk between Dll1$^+$ tumor cells and CAFs contributes to radioresistance in patient derived xenograft (PDX) samples, which mimic human breast cancer very closely [47]. We used two ER$^+$/PR$^+$ PDX tumors, HCI-013 and HCI-032, derived from ER$^+$ luminal breast cancer patients [48] (Supplementary Fig. S12A). Notably, HCI-032 with higher Dll1 protein shows a significant increase in tumor growth compared to HCI-013 (lower Dll1 at baseline), suggesting that HCI-032 is more aggressive (Fig. 7A; Supplementary Fig. S12B). Moreover, H&E images demonstrated an increased abundance of macronuclear tumor cells and higher abundance of dense stroma in HCI-032 compared to HCI-013, which was further confirmed by IF and IHC showing more abundant single αSMA$^+$ cells and FAP$^+$ cells in aggressive HCI-032 tumors than in HCI-013 (Supplementary Fig. S12C–S12G). In addition, nuclear localization of β-catenin was increased in HCI-032 tumors relative to HCI-013, suggesting that some Wnt signaling may be activated in HCI-032 PDX tumors (Supplementary Fig. S12H). Of note, HCI-032 PDX tumor cells also form more tumorspheres compared to HCI-013 in suspension culture *in vitro* (Supplementary Fig. 12I and S12J), suggesting the presence of more functional CSCs. To further examine if addition of CAFs might facilitate stem cell functions post radiation, PDX tumors were cultured alone or in combination with sorted CAFs (EPCAM$^-$PDGFRα$^+$) from fresh ER$^+$/PR$^+$ human patient tumors and were subjected to irradiation as shown in the schematic diagram (Supplementary Fig. S12A). Western blot data revealed that DLL1 protein was expressed more highly in aggressive HCI-032 compared to HCI-013 after radiation (Fig. 7A and Supplementary Fig. S13). More importantly, clonogenic survival assay showed a significant increase in cell viability of HCI-032 tumor cells with CM from human sorted CAFs in short term culture compared to HCI-013 tumor cells co-cultured with CAFs post radiation, suggesting HCI-032 are more aggressive and radioresistant than HCI-013 (Supplementary Fig. S12K). Furthermore, a significantly greater number of tumorspheres and nuclear localization of β-catenin were observed by HCI-032 PDX tumors (DLL1^{high}) co-cultured with CAFs following radiation compared to HCI-013 PDX tumors (DLL1^{lo}) co-cultured with CAFs, suggesting that HCI-032 PDX tumor cells with high DLL1 have more stem cell properties and upregulation of Wnt signaling post radiation in presence of CAFs (Fig. 7B–E). Taken together, these data strongly corroborate our mouse data and suggest CAFs play a crucial role in Dll1-mediated promotion of CSC function that contributes to radioresistance in luminal breast cancer.

Furthermore, Wnt reporter assay with stable PDX cell lines (HCI-013–7TGC and HCI-032–7TGC) using the lentiviral based Wnt-reporter, 7TGC plasmid [46] confirmed that activation of Wnt signaling based on increase in mCherry$^+$/GFP$^+$ expression was increased in HCI-032–7TGC PDX tumor cells compared to HCI-013–7TGC PDX tumor cells when co-cultured with CAFs post radiation (Fig. 7F and G). Pharmacological blocking of Notch signaling using DAPT or anti-DLL1 antibody or inhibiting Wnt signaling using JW-74 significantly reduced tumorsphere number post radiation in HCI-032 PDX tumor cells compared to untreated HCI-032 PDX tumors (Fig. 7H and I). More importantly, prevention of Wnt ligand secretion by LGK-974 post radiation significantly decreased tumorsphere

number of HCI-032 PDX tumor cells (Fig. 7H and I) and Wnt target genes expression as evidenced by qPCR (Fig. 7J), further reinforcing our *in vitro* data. Taken together, our data suggest that blocking Wnt signaling or Dll1 mediated Notch signaling reverses the increase in stemness during radioresistance (Fig. 7K).

Discussion

Breast cancer is a deadly form of cancer among women worldwide [49]. Consequently, advances in the treatment of this cancer are of the highest priority. The efficacy of RT, a major treatment modality for breast cancer, is severely attenuated by emergence of radioresistance, but the underlying mechanism is not fully understood. Recent evidence points to a strong correlation between Notch receptors and radioresistance in several cancers [50, 51], including breast cancer [52]. Additional preclinical studies have also shown that CSCs have a radiation-resistant phonotype, and that radiation treatment enriches for the CSC population [53]. However, the functional impact of Notch signaling on CSCs during radioresistance is not clear. Our present study reveals a central role for the Notch ligand Dll1 in promoting radioresistance. We found increased expression of DLL1 in NART patient tumors, suggesting that radiation may augment $DLL1^+$ CSCs in these patients, thereby potentially contributing to radioresistance. Furthermore, an increased abundance of FAP and αSMA expressing CAFs in luminal ER^+/PR^+ patient tumors post radiation indicated a possible crosstalk between $DLL1^+$ CSC and CAFs to promote resistance to RT in breast cancer patients. This high prognostic capability of DLL1 and CAFs is limited to NART ER^+/PR^+ patients, based on the current study. However, the number of ART patient tumor samples were too low to reach statistical significance for DLL1, although the correlation for myCAFs (αSMA^+), but not activated FAP^+ CAFs holds true in this small number of patient samples. In the future, larger sample size of ER^+/PR^+ patient samples in both NART and ART settings need to be evaluated to determine if the number of DLL1 cells and CAFs can be used as biomarker to identify patients at high-risk for radioresistance. Additional studies assessing DLL1 expression prior to NART may also reveal if RT should be avoided all together in patients with high basal levels of DLL1 expression or if concomitant administration of DLL1-targeted therapeutics is warranted to improve prognosis.

CAFs comprise the most dominant population within the breast cancer TME and can contribute to drug resistance. However, functional analysis of this heterogeneous population remains challenging. Our scRNA-seq data show that activated FAP^+ CAFs and αSMA^+ myCAF populations are increased in $Dll1^+$ tumors. Furthermore, conditional knockout of Dll1 in tumor cells reduces the number of FAP^+ and αSMA^+ CAF subpopulations, suggesting that Dll1 is responsible for quantitative and qualitative alterations in CAF abundance. We also observed $Dll1^+$ cells became more hypoxic post radiation in murine primary breast tumors. Notably, disseminated $Dll1^+$ cells were significantly higher in the blood of irradiated mice after radiation, suggesting that hypoxic $Dll1^+$ tumor cells disseminate after radiation, potentially contributing to distal organ metastasis. Shedding of tumor cells post radiation is well known in cancer [54] and DTCs can contribute to metastasis at distal sites. Our data suggest that hypoxic $Dll1^+$ tumor cells and excess $Dll1^+$ DTCs likely contribute to metastasis. Future studies involving other luminal breast cancer models and human tumor cells will be needed to examine the causal role of $Dll1^+$ tumor

cells on metastasis post radiation. Additionally, other upcoming studies will determine if therapeutic targeting of these cells will decrease radioresistance and metastatic disease.

IL-6 is involved in several cancer-associated fibroblasts and clinical studies have shown that high serum IL-6 levels are indicative of poor prognosis and survival in breast and other cancers [55]. IL-6 induces EMT by activating the JAK-STAT3-SNAIL pathway [56]. Although IL-6 secreted from CAFs can contribute to therapeutic resistance [57], the function of breast tumor secreted IL-6 on CAFs remains unexplored. Mechanistically, we show that $Dll1^{+}$ tumor cells secrete IL-6 to promote recruitment of CAFs after radiation. CAFs from irradiated tumors showed increased expression of *Notch2* and *Notch3* as well as Notch target genes such as *Hes2* and *HeyL,* suggesting that Dll1 mediated Notch signaling activation occurs after CAF recruitment to the TME post radiation. Our data demonstrated that blockade of IL-6 and Dll1-Notch signaling significantly reverts this process and makes tumor sensitive to radiation suggesting that IL-6 from the tumor cells have a critical role in Dll1-dependent recruitment of CAFs and acquisition of radioresistance in breast cancer. Mechanistically, we also show that Dll1 driven radio resistance is reactive oxygen species (ROS) dependent as viability of $Dll1^{high}$ CSCs can be reduced by addition of exogenous antioxidant enzyme, catalase. It has been reported that ROS plays a vital role in modulating drug resistant CSCs [53, 58]. Our study indicates that high intracellular ROS production in irradiated $Dll1^{+}$ cancer cells along with CAFs may lead to radio resistance.

CAFs are associated with immune-suppression and resistance as well as promotion of stem cell properties in multiple cancers, including breast [59]. CAFs secrete TGF-β1 and osteopontin (OPN) to induce EMT and enhance CSC function [60–62]. In human breast cancer, $CD24^{-}CD44^{+}$ cells show CSC function and high tumorigenicity. This stem cell phenotype is dependent on both canonical and noncanonical Wnt signaling [42]. Here, we present data supporting a novel mechanism by which CAFs influence CSC function post radiation. Specifically, we show that activation of Dll1 mediated Notch signaling in CAFs upregulates the secretion of Wnt ligands, thereby activating Wnt signaling in CSCs. Notably, blocking Wnt secretion from CAFs using a clinically tested drug LGK-974 reverts this phenotype, opening new possible avenues of treatment of patients with radioresistant breast cancer.

To corroborate our findings from mouse and human clinical data, we used breast cancer PDX models that accurately mimic the heterogeneity of the tumors of origin to decipher the intricate radiation induced crosstalk between tumor cells and CAFs. Higher expression of DLL1 protein in radioresistant PDX tumor cells, suggests DLL1 mediated Notch signaling may promote radioresistance of breast tumor cells corroborating mouse tumor data. Furthermore, nuclear translocation of β-catenin in tumor cells in response to Wnt ligand secretion by CAFs suggests activated Wnt signaling in PDX tumor cells when co-cultured with CAFs. In support, use of Wnt signaling inhibitors such as JW-74 or LGK-974 or inhibition of Notch signaling using GSI (DAPT) or anti-DLL1 blocking antibody reverts the stem cell phenotype, strongly suggesting an indispensable role for the Dll1 mediated Notch pathway in promoting Wnt signaling in $Dll1^{+}$ CSCs to drive radioresistance.

In summary, our study sheds light on a novel crosstalk between Dll1-Notch and Wnt signaling between $Dll1^+$ tumor cells and CAFs that promotes radioresistance (Fig. 7K), which may be further exploited in the near future as an alternative therapeutic application aimed to revert radioresistance in breast cancer patients.

Supplementary Material

Refer to Web version on PubMed Central for supplementary material.

Acknowledgements

We thank Dr. Leslie King and Snahlata Singh (School of Veterinary Medicine, University of Pennsylvania) and Dr. Ioannis I. Verginadis (Perelman University School of Medicine, University of Pennsylvania) for critical comments and helpful discussions. We thank Dr. Ellen Pure for FAP antibodies used in flow cytometry analyses and helpful discussions. We thank Dr. Christian W. Siebel for providing anti-DLL1 antibody and critical comments. We thank Eastern Division of the Cooperative Human Tissue Network (CHTN), UPENN for providing human breast cancer fixed tissues and fresh tumor tissues from patients. We thank Penn Vet Comparative Pathology Core, Children's Hospital of Philadelphia (CHOP) histology core and Perelman School of Medicine histology core for their assistance with embedding and sectioning of tumor samples and Penn Vet imaging core for providing confocal microscopy service. We also thank the members of SARRP radiation machine in Department of Radiation Oncology, Flow Cytometry core at UPENN and Children's Hospital of Philadelphia (CHOP) for all flow-based experiments. We thank to PSOM Next-Generation Sequencing Core for running single cell RNA sequencing. We also thank Novogene Corporation, Inc. for bulk mRNA sequencing and analyses. Generation of human PDX tumors was supported by NCI U54CA224076 to A.L.W. and Department of Defense Breast Cancer Research Program Era of Hope Scholar Award W81XWH1210077 to A. L. W. This work was supported by grants from American Cancer Society (RSG DDC-133604), Emerson Collective Fund-University of Pennsylvania (20200315113131) and NCI-R01 (R01CA237243) grants to R.C.

References

1. But-Hadzic J, Bilban-Jakopin C, and Hadzic V, The role of radiation therapy in locally advanced breast cancer. Breast J, 2010. 16(2): p. 183–8. [PubMed: 20030645]
2. Gera R, et al. , Locoregional therapy of the primary tumour in de novo stage IV breast cancer in 216 066 patients: A meta-analysis. Sci Rep, 2020. 10(1): p. 2952. [PubMed: 32076063]
3. Loganadane G, et al. , [Locoregional control and patterns of locoregional failure in women with breast cancer treated by highly conformal electron beam irradiation]. Cancer Radiother, 2019. 23(1): p. 38–45. [PubMed: 30595340]
4. Choi J, et al. , Predicting Radiation Resistance in Breast Cancer with Expression Status of Phosphorylated S6K1. Sci Rep, 2020. 10(1): p. 641. [PubMed: 31959810]
5. Barker HE, et al. , The tumour microenvironment after radiotherapy: mechanisms of resistance and recurrence. Nat Rev Cancer, 2015. 15(7): p. 409–25. [PubMed: 26105538]
6. Kalluri R, The biology and function of fibroblasts in cancer. Nat Rev Cancer, 2016. 16(9): p. 582–98. [PubMed: 27550820]
7. Bartoschek M, et al. , Spatially and functionally distinct subclasses of breast cancer-associated fibroblasts revealed by single cell RNA sequencing. Nat Commun, 2018. 9(1): p. 5150. [PubMed: 30514914]
8. Hanahan D and Coussens LM, Accessories to the crime: functions of cells recruited to the tumor microenvironment. Cancer Cell, 2012. 21(3): p. 309–22. [PubMed: 22439926]
9. Steer A, et al. , Impact of Cancer-Associated Fibroblast on the Radiation-Response of Solid Xenograft Tumors. Front Mol Biosci, 2019. 6: p. 70. [PubMed: 31475157]
10. Ohuchida K, et al. , Radiation to stromal fibroblasts increases invasiveness of pancreatic cancer cells through tumor-stromal interactions. Cancer Res, 2004. 64(9): p. 3215–22. [PubMed: 15126362]
11. Tommelein J, et al. , Cancer-associated fibroblasts connect metastasis-promoting communication in colorectal cancer. Front Oncol, 2015. 5: p. 63. [PubMed: 25853091]

12. Meurette O and Mehlen P, Notch Signaling in the Tumor Microenvironment. Cancer Cell, 2018. 34(4): p. 536–548. [PubMed: 30146333]
13. Nandi A and Chakrabarti R, The many facets of Notch signaling in breast cancer: toward overcoming therapeutic resistance. Genes Dev, 2020. 34(21–22): p. 1422–1438. [PubMed: 33872192]
14. Ranganathan P, Weaver KL, and Capobianco AJ, Notch signalling in solid tumours: a little bit of everything but not all the time. Nat Rev Cancer, 2011. 11(5): p. 338–51. [PubMed: 21508972]
15. Kumar S, et al. , Estrogen-dependent DLL1-mediated Notch signaling promotes luminal breast cancer. Oncogene, 2019. 38(12): p. 2092–2107. [PubMed: 30442981]
16. Kumar S, et al. , Dll1(+) quiescent tumor stem cells drive chemoresistance in breast cancer through NF-kappaB survival pathway. Nat Commun, 2021. 12(1): p. 432. [PubMed: 33462238]
17. Shackleton M, et al. , Generation of a functional mammary gland from a single stem cell. Nature, 2006. 439(7072): p. 84–8. [PubMed: 16397499]
18. Chakrabarti R, et al. , DeltaNp63 promotes stem cell activity in mammary gland development and basal-like breast cancer by enhancing Fzd7 expression and Wnt signalling. Nat Cell Biol, 2014. 16(10): p. 1004–15, 1–13. [PubMed: 25241036]
19. Zhuang Y, et al. , Establishment and characterization of immortalized human breast cancer cell lines from breast cancer patient-derived xenografts (PDX). NPJ Breast Cancer, 2021. 7(1): p. 79. [PubMed: 34145270]
20. Chakrabarti R, et al. , Notch ligand Dll1 mediates cross-talk between mammary stem cells and the macrophageal niche. Science, 2018. 360(6396).
21. Cheung KJ, et al. , Collective invasion in breast cancer requires a conserved basal epithelial program. Cell, 2013. 155(7): p. 1639–51. [PubMed: 24332913]
22. Sebastian A, et al. , Single-Cell Transcriptomic Analysis of Tumor-Derived Fibroblasts and Normal Tissue-Resident Fibroblasts Reveals Fibroblast Heterogeneity in Breast Cancer. Cancers (Basel), 2020. 12(5).
23. Vaidya JS, et al. , Targeted intraoperative radiotherapy versus whole breast radiotherapy for breast cancer (TARGIT-A trial): an international, prospective, randomised, non-inferiority phase 3 trial. Lancet, 2010. 376(9735): p. 91–102. [PubMed: 20570343]
24. Hara T, et al. , Metastasis of breast cancer cells to the bone, lung, and lymph nodes promotes resistance to ionizing radiation. Strahlenther Onkol, 2017. 193(10): p. 848–855. [PubMed: 28642964]
25. Feys L, et al. , Radiation-induced lung damage promotes breast cancer lung-metastasis through CXCR4 signaling. Oncotarget, 2015. 6(29): p. 26615–32. [PubMed: 26396176]
26. Sai B and Xiang J, Disseminated tumour cells in bone marrow are the source of cancer relapse after therapy. J Cell Mol Med, 2018. 22(12): p. 5776–5786. [PubMed: 30255991]
27. Aguirre-Ghiso JA, Models, mechanisms and clinical evidence for cancer dormancy. Nat Rev Cancer, 2007. 7(11): p. 834–46. [PubMed: 17957189]
28. Chambers AF, Groom AC, and MacDonald IC, Dissemination and growth of cancer cells in metastatic sites. Nat Rev Cancer, 2002. 2(8): p. 563–72. [PubMed: 12154349]
29. Lytle NK, Barber AG, and Reya T, Stem cell fate in cancer growth, progression and therapy resistance. Nat Rev Cancer, 2018. 18(11): p. 669–680. [PubMed: 30228301]
30. Al-Hajj M, et al. , Prospective identification of tumorigenic breast cancer cells. Proc Natl Acad Sci U S A, 2003. 100(7): p. 3983–8. [PubMed: 12629218]
31. Costa A, et al. , Fibroblast Heterogeneity and Immunosuppressive Environment in Human Breast Cancer. Cancer Cell, 2018. 33(3): p. 463–479 e10. [PubMed: 29455927]
32. Semenza GL, Hypoxia-inducible factors: coupling glucose metabolism and redox regulation with induction of the breast cancer stem cell phenotype. EMBO J, 2017. 36(3): p. 252–259. [PubMed: 28007895]
33. Yamada D, et al. , Role of crosstalk between interleukin-6 and transforming growth factor-beta 1 in epithelial-mesenchymal transition and chemoresistance in biliary tract cancer. Eur J Cancer, 2013. 49(7): p. 1725–40. [PubMed: 23298711]

34. Yao Z, et al. , TGF-beta IL-6 axis mediates selective and adaptive mechanisms of resistance to molecular targeted therapy in lung cancer. Proc Natl Acad Sci U S A, 2010. 107(35): p. 15535–40. [PubMed: 20713723]
35. Li X, et al. , CXCL12/CXCR4 pathway orchestrates CSC-like properties by CAF recruited tumor associated macrophage in OSCC. Exp Cell Res, 2019. 378(2): p. 131–138. [PubMed: 30857971]
36. Trinchieri G, Interleukin-12 and the regulation of innate resistance and adaptive immunity. Nat Rev Immunol, 2003. 3(2): p. 133–46. [PubMed: 12563297]
37. Noman AS, et al. , Serum sonic hedgehog (SHH) and interleukin-(IL-6) as dual prognostic biomarkers in progressive metastatic breast cancer. Sci Rep, 2017. 7(1): p. 1796. [PubMed: 28496132]
38. Caetano MS, et al. , IL6 Blockade Reprograms the Lung Tumor Microenvironment to Limit the Development and Progression of K-ras-Mutant Lung Cancer. Cancer Res, 2016. 76(11): p. 3189–99. [PubMed: 27197187]
39. Karkera J, et al. , The anti-interleukin-6 antibody siltuximab down-regulates genes implicated in tumorigenesis in prostate cancer patients from a phase I study. Prostate, 2011. 71(13): p. 1455–65. [PubMed: 21321981]
40. Lu L, et al. , Activation of STAT3 and Bcl-2 and reduction of reactive oxygen species (ROS) promote radioresistance in breast cancer and overcome of radioresistance with niclosamide. Oncogene, 2018. 37(39): p. 5292–5304. [PubMed: 29855616]
41. Su S, et al. , CD10(+)GPR77(+) Cancer-Associated Fibroblasts Promote Cancer Formation and Chemoresistance by Sustaining Cancer Stemness. Cell, 2018. 172(4): p. 841–856 e16. [PubMed: 29395328]
42. Yin P, et al. , Wnt signaling in human and mouse breast cancer: Focusing on Wnt ligands, receptors and antagonists. Cancer Sci, 2018. 109(11): p. 3368–3375. [PubMed: 30137666]
43. Griffin JN, et al. , RAPGEF5 Regulates Nuclear Translocation of beta-Catenin. Dev Cell, 2018. 44(2): p. 248–260 e4. [PubMed: 29290587]
44. Waaler J, et al. , Novel synthetic antagonists of canonical Wnt signaling inhibit colorectal cancer cell growth. Cancer Res, 2011. 71(1): p. 197–205. [PubMed: 21199802]
45. Liu J, et al. , Targeting Wnt-driven cancer through the inhibition of Porcupine by LGK974. Proc Natl Acad Sci U S A, 2013. 110(50): p. 20224–9. [PubMed: 24277854]
46. Fuerer C and Nusse R, Lentiviral vectors to probe and manipulate the Wnt signaling pathway. PLoS One, 2010. 5(2): p. e9370. [PubMed: 20186325]
47. Dobrolecki LE, et al. , Patient-derived xenograft (PDX) models in basic and translational breast cancer research. Cancer Metastasis Rev, 2016. 35(4): p. 547–573. [PubMed: 28025748]
48. Sikora MJ, et al. , Invasive lobular carcinoma cell lines are characterized by unique estrogen-mediated gene expression patterns and altered tamoxifen response. Cancer Res, 2014. 74(5): p. 1463–74. [PubMed: 24425047]
49. Senkus E, et al. , Primary breast cancer: ESMO Clinical Practice Guidelines for diagnosis, treatment and follow-up. Ann Oncol, 2015. 26 Suppl 5: p. v8–30. [PubMed: 26314782]
50. Theys J, et al. , High NOTCH activity induces radiation resistance in non small cell lung cancer. Radiother Oncol, 2013. 108(3): p. 440–445. [PubMed: 23891097]
51. Wang J, et al. , Notch promotes radioresistance of glioma stem cells. Stem Cells, 2010. 28(1): p. 17–28. [PubMed: 19921751]
52. Ko YS, et al. , Radioresistant breast cancer cells exhibit increased resistance to chemotherapy and enhanced invasive properties due to cancer stem cells. Oncol Rep, 2018. 40(6): p. 3752–3762. [PubMed: 30272295]
53. Diehn M, et al. , Association of reactive oxygen species levels and radioresistance in cancer stem cells. Nature, 2009. 458(7239): p. 780–3. [PubMed: 19194462]
54. Liu Y, et al. , Radiotherapy targeting cancer stem cells “awakens” them to induce tumour relapse and metastasis in oral cancer. Int J Oral Sci, 2020. 12(1): p. 19. [PubMed: 32576817]
55. Lukaszewicz M, Mroczko B, and Szmitkowski M, [Clinical significance of interleukin-6 (IL-6) as a prognostic factor of cancer disease]. Pol Arch Med Wewn, 2007. 117(5–6): p. 247–51. [PubMed: 18030875]

56. Yadav A, et al. , IL-6 promotes head and neck tumor metastasis by inducing epithelial-mesenchymal transition via the JAK-STAT3-SNAIL signaling pathway. Mol Cancer Res, 2011. 9(12): p. 1658–67. [PubMed: 21976712]

57. Mao Y, et al. , Stromal cells in tumor microenvironment and breast cancer. Cancer Metastasis Rev, 2013. 32(1–2): p. 303–15. [PubMed: 23114846]

58. Gorrini C, Harris IS, and Mak TW, Modulation of oxidative stress as an anticancer strategy. Nat Rev Drug Discov, 2013. 12(12): p. 931–47. [PubMed: 24287781]

59. Houthuijzen JM and Jonkers J, Cancer-associated fibroblasts as key regulators of the breast cancer tumor microenvironment. Cancer Metastasis Rev, 2018. 37(4): p. 577–597. [PubMed: 30465162]

60. Sahai E, et al. , A framework for advancing our understanding of cancer-associated fibroblasts. Nat Rev Cancer, 2020. 20(3): p. 174–186. [PubMed: 31980749]

61. Chen X and Song E, Turning foes to friends: targeting cancer-associated fibroblasts. Nat Rev Drug Discov, 2019. 18(2): p. 99–115. [PubMed: 30470818]

62. Yu Y, et al. , Cancer-associated fibroblasts induce epithelial-mesenchymal transition of breast cancer cells through paracrine TGF-beta signalling. Br J Cancer, 2014. 110(3): p. 724–32. [PubMed: 24335925]

Significance

Dll1^{+} breast cancer cells activate Notch signaling in cancer-associated fibroblasts that increases Wnt ligand secretion and leads to β-catenin-driven radioresistance and metastasis, opening new therapeutic avenues for breast cancer.

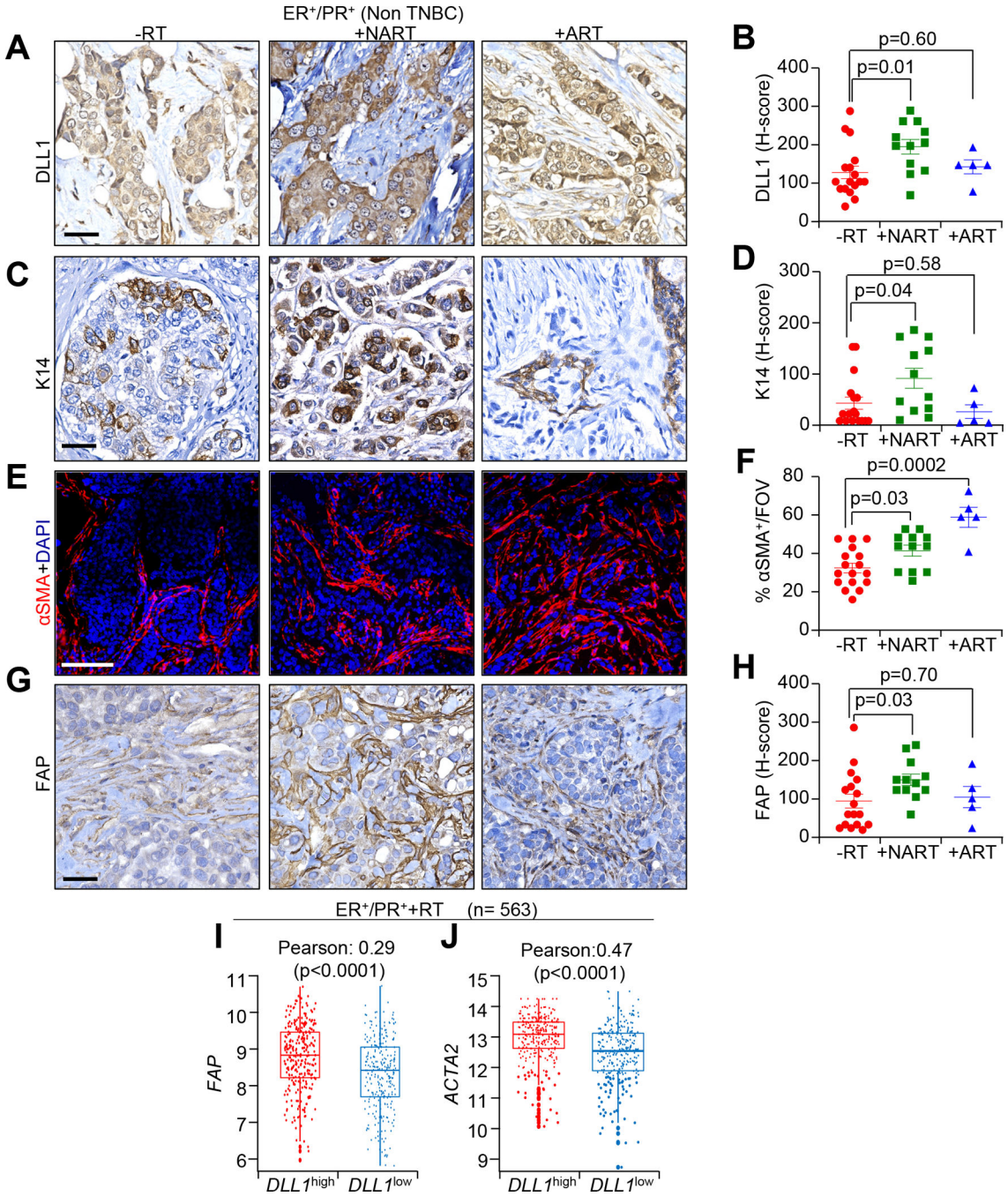

Figure 1.

Radiation increases the expression of DLL1 in tumor cells and FAP$^+$ and αSMA$^+$ CAFs in ER$^+$/PR$^+$ luminal breast cancer patients following RT. **A-D,** IHC images and H-score quantification of DLL1 (**A** and **B**) and K14 (**C** and **D**), **E,** IF images and **F,** quantification of αSMA **G,** IHC images and **H,** H-score quantification of FAP in radiation untreated (-RT), neoadjuvant radiation treated (NART) and adjuvant radiation treated (ART) luminal patient tumors. The dots in each scatter plot represent each patient tumor/group. (n=17 for -RT; n=12 +NART and n=5 +ART tumors). **I** and **J,** METABRIC dataset demonstrates correlation

between *DLL1* (**I**) and *ACTA2* (**J**) expression in +RT ER^+/PR^+ (n=563) luminal breast cancer patients. Data are presented as the mean ± SEM. FOV stands for field of view. Unpaired student's *t* test was used to calculate p values. Scale bars, 100 μM.

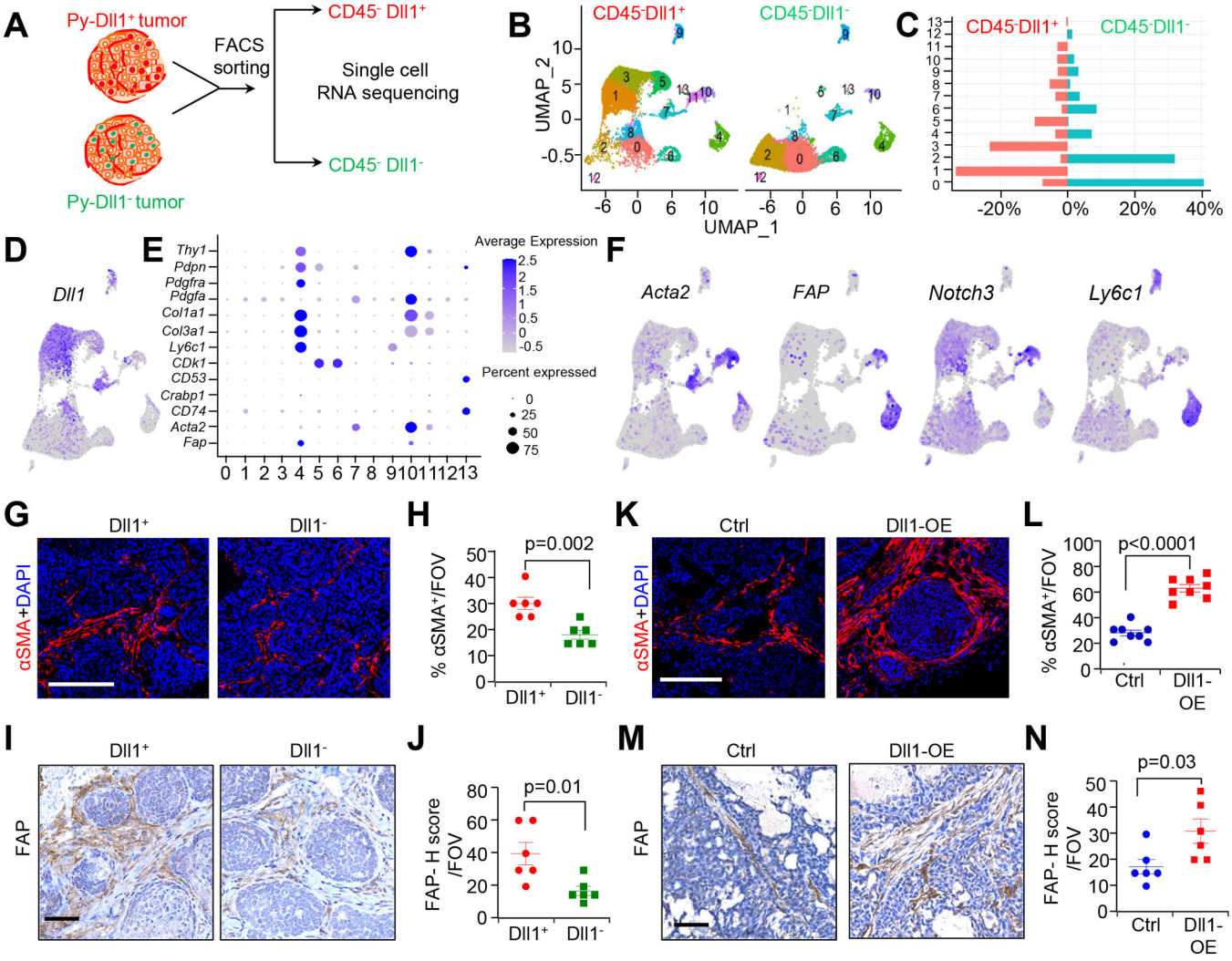

Figure 2.

Single cell sequencing (scRNA-seq) data show increase in myCAF population in Dll1$^+$ luminal breast tumors. **A,** Schematic strategy of scRNA-seq of CD45$^-$ Dll1$^+$ and Dll1$^-$ cells from Py-Dll1$^+$ and Py-Dll1$^-$ tumors. **B,** UMAP embedding shows distribution of total CD45$^-$ cells from both Dll1$^+$ and Dll1$^-$ breast tumors. **C,** Bar graph depicts percent distribution of Py-Dll1$^+$ and Py-Dll1$^-$ tumor cells within each cluster. **D,** Feature plot shows higher expression of *Dll1* in clusters 1, 3, 5 and 8. **E,** Dot plot shows the expression of selected CAF markers in different CD45$^-$ clusters. **F,** Feature plots show CAF sub populations, based on *Acta2*, *FAP, Notch3* and *Ly6c1* expression. **G-J,** IF and IHC images and quantification of αSMA$^+$ cells (**G** and **H**) and FAP$^+$ cells (**I** and **J**) in Dll1$^+$ and Dll1$^-$ breast tumors. **K-N,** IF and IHC images and quantification of αSMA$^+$ cells (**K** and **L**) and FAP$^+$ cells (**M** and **N**) in Dll1 over-expressing (OE) and control (vector) WTB xenograft tumors [15]. Insets (**I** and **M**) showing zoomed-in image. The dots in scatter plot represent the field of view (FOV), n=4 tumors/group. Data are presented as the mean ± SEM. Unpaired student's *t* test was used to calculate p values. Scale bars, 100 μm.

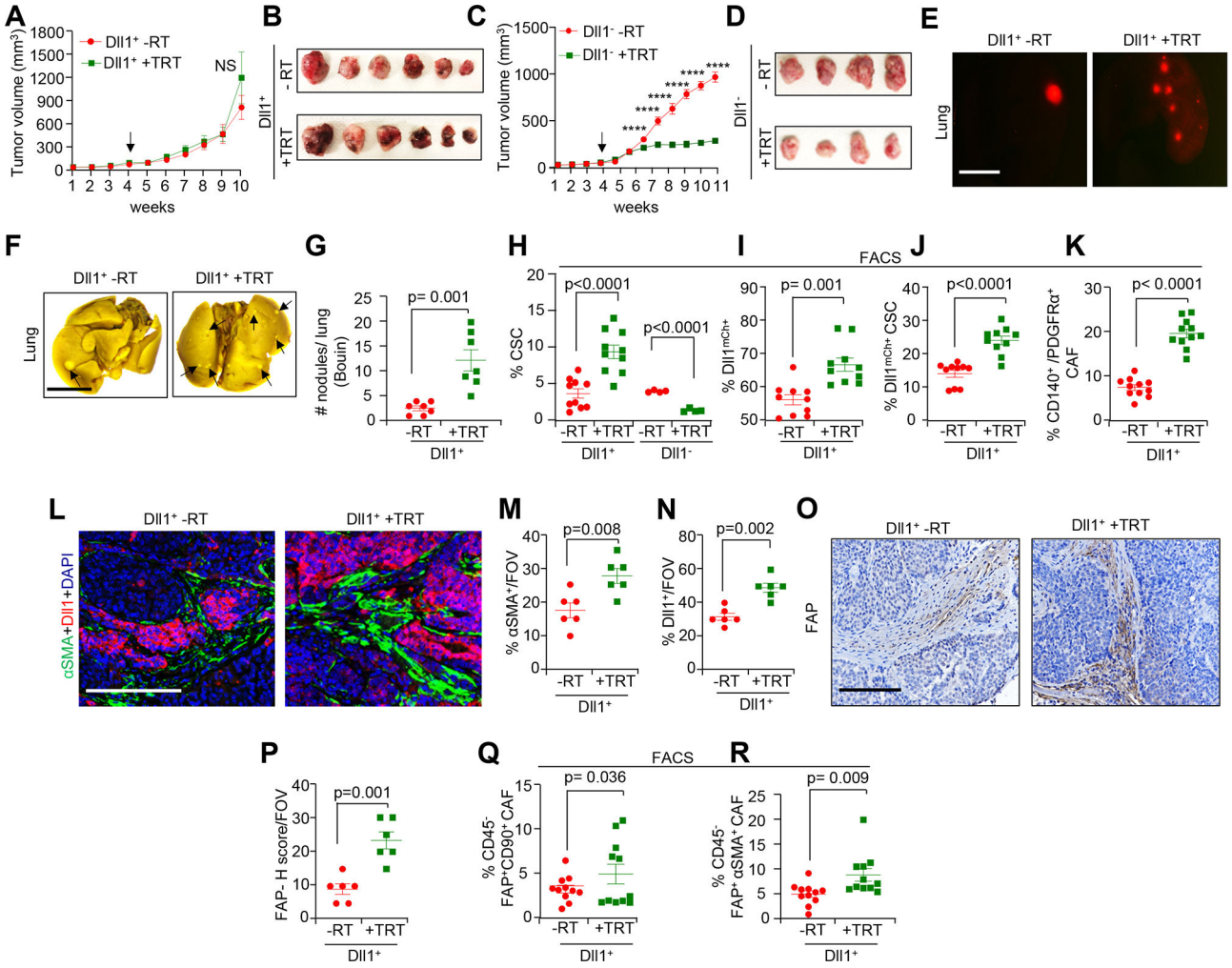

Figure 3.

Radiation increases Dll1^{+} CSCs and CAFs in Dll1^{+} luminal breast tumors. A total of 80,000 sorted Dll1^{+} and Dll1^{-} tumor cells from Py-Dll1^{mCh} spontaneous tumors were orthotopically injected into syngeneic C57BL/6 mice. TRT (6 Gy) was given when tumors were established (indicated by black arrow) and tumors (n= 8 tumors/group for Dll1^{+} tumors, data was combined from two independent experiments) and (n=6 tumors/group for Dll1^{-} tumors) were harvested ~6–7 weeks later. The experiment was repeated twice. **A-D,** Tumor growth curve and whole tumor images, from Dll1^{+} tumors (**A** and **B**) and Dll1^{-} tumors (**C** and **D**) after TRT. **E,** Fluorescence images showing a greater number Dll1^{mCh} cells in +TRT Dll1^{+} whole lungs compared to -RT lung. (**F** and **G**), Whole lung images post Bouin fixation (**F**) and quantification (**G**) showing a greater number of metastatic nodules (indicated by black arrows) in +TRT Dll1^{+} lungs. Data is combined from two independent experiments (n=7 mice/group). (**H-J),** Flowcytometry graphs showing increased CSC (CD24^{-}CD44^{+}) population (**H**), Dll1^{mCh+} tumor cells (**I**) and double positive Dll1^{mCh+} CSC (Dll1$^{mCherry+}$CD24^{-}CD44^{+}) populations (**J**) in Dll1^{+} tumors after TRT. **K,** Flowcytometry analysis showing an increased CD140^{+}/PDGFRα^{+} CAF population in +TRT Dll1^{+} tumors. Data is combined from two independent experiments. **(L-N),** IF

images (**L**) and scatter plots (**M** and **N**) showing increased αSMA$^+$ CAFs and Dll1$^+$ tumor cells in Dll1$^+$ primary tumors after TRT. **(O-R),** IHC images and quantification (**O and P**) showing increased abundance of FAP$^+$ CAFs, and Flowcytometry data showing FAP$^+$ CD90$^+$ CAF (CD45$^-$FAP$^+$CD90$^+$) subpopulation (**Q**) and FAP$^+$ αSMA expressing myCAF subpopulation (CD45$^-$FAP$^+$αSMA$^+$) (**R**) in +TRT Dll1$^+$ tumors than -RT tumors. Data was combined from two independent experiments. Each dot in the scatter plot (**H-K** and **Q-R**) represents an individual tumor. The dots in the scatter plot (**M**, **N** and **P**) represent the field of views (FOVs) from n=4 tumors/group. Data are presented as the mean ± SEM. Two-way ANOVA with Bonferroni post-test (**A, C**) and unpaired student's *t* test (**G-K, M-N, P-R**) were used to calculate p values. *p < 0.05, ***p < 0.001, ****p < 0.0001. Scale bars, 100 μm (**L** and **O**) and 4 mm (**E** and **F**).

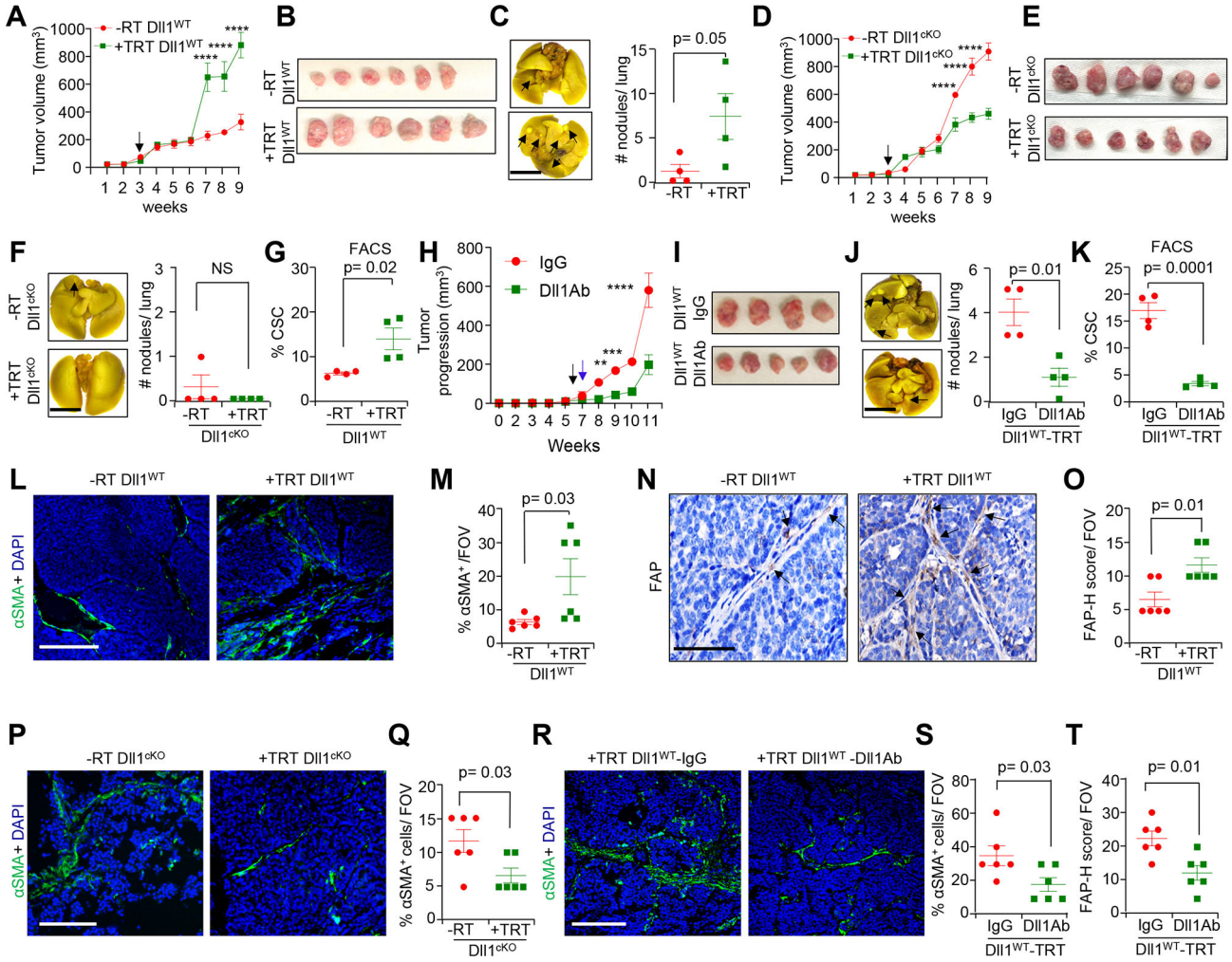

Figure 4.

Genetic and pharmacological blocking of Dll1 reveals indispensable role of Dll1 in tumor progression, lung metastasis and infiltration of αSMA^{+} myCAFs in luminal tumors post radiation. **(A** and **B),** Tumor growth curve (**A**); and representative whole tumor images (**B**) showing increased tumor progression in Py-Dll1^{WT} tumors after TRT (n=6 tumors/group). **C,** A representative whole mount lung image (left panel) and scatter plot (right panel) showing a greater number of metastatic nodules (black arrows) in Py-Dll1^{WT} lungs upon TRT. (**D** and **E),** Tumor growth curve (**D**); and representative whole tumor images (**E**) showing slower tumor progression Py-Dll1^{cKO} tumors after TRT (n=6 tumors/group). A total of 70,000 sorted tumor cells from Py-Dll1$^{WT/cKO}$ mice were orthotopically injected into the mammary fat pad (MFP) of C57/BL6 mice. Black arrow indicates day of TRT. **F,** A representative whole mount lung image (left panel) and scatter plot (right panel) showing no difference in metastatic nodules (black arrows) in Py-Dll1^{cKO} mice with and without TRT. **G,** Flowcytometry analysis depicting an increase in the number of cancer stem cells (CSCs) in Py-Dll1^{WT} primary tumors after TRT compared to -RT. (**H** and **I),** Tumor progression curve (**H**); and representative whole tumor images (**I**) showing tumor growth was slower in +TRT Py-Dll1^{WT} mice injected with anti-Dll1-blocking antibody

(18 mg/kg) compared with those treated with anti-IgG control antibody (n=4 tumors for IgG and n=4 tumors for Dll1 blocking antibody). A total of 40,000 sorted primary tumor cells from Py-Dll1^{WT} were injected into the MFP of C57BL/6 mice. Drug was given every alternate day. Black arrow indicates day of TRT. Blue arrow indicates starting time of treatments. **J,** A representative whole mount lung image (left panel) and scatter plot (right panel) showing reduced metastatic nodules (black arrows) in anti- Dll1 blocking antibody treated lung. **K,** Flowcytometry analysis showing decreased numbers of CSCs in anti-Dll1-blocking antibody treated +TRT Py-Dll1^{WT} primary tumors (n=4 tumors/ group). (L-O) Representative IF images and quantification (**L** and **M),** and IHC images and quantification (**M** and **N**) showing increased αSMA^{+} and FAP^{+} cells, in Py-Dll1^{WT} primary tumors upon TRT. **P,** Representative IF images and **Q,** quantification showing decreased αSMA^{+} cells in +TRT Py-Dll1^{cKO} primary tumors. (**R-T),** Representative IF images (**R**) and quantification showing decreased αSMA^{+} cells (**S**) and decreased FAP^{+} cells (based on H-score) (**T**) in +TRT Py-Dll1^{WT} primary tumors upon anti Dll1-blocking antibody treatment compared to IgG treated tumors. The dots in scatter plot represent the field of views (FOVs), n=4 tumors/group. This experiment was performed twice. Data are presented as the mean ± SEM. Two-way ANOVA with Bonferroni post-test (**A, D, H**) and unpaired student's *t* test (**C, F, G, J-K, M, O, Q, S and T**) were used to calculate p values. ** p<0.01, ***p < 0.001 and **** p<0.0001. Scale bars, 4mm (**C, F** and **J**) and 100 μm (**L, N**, **P** and **R**).

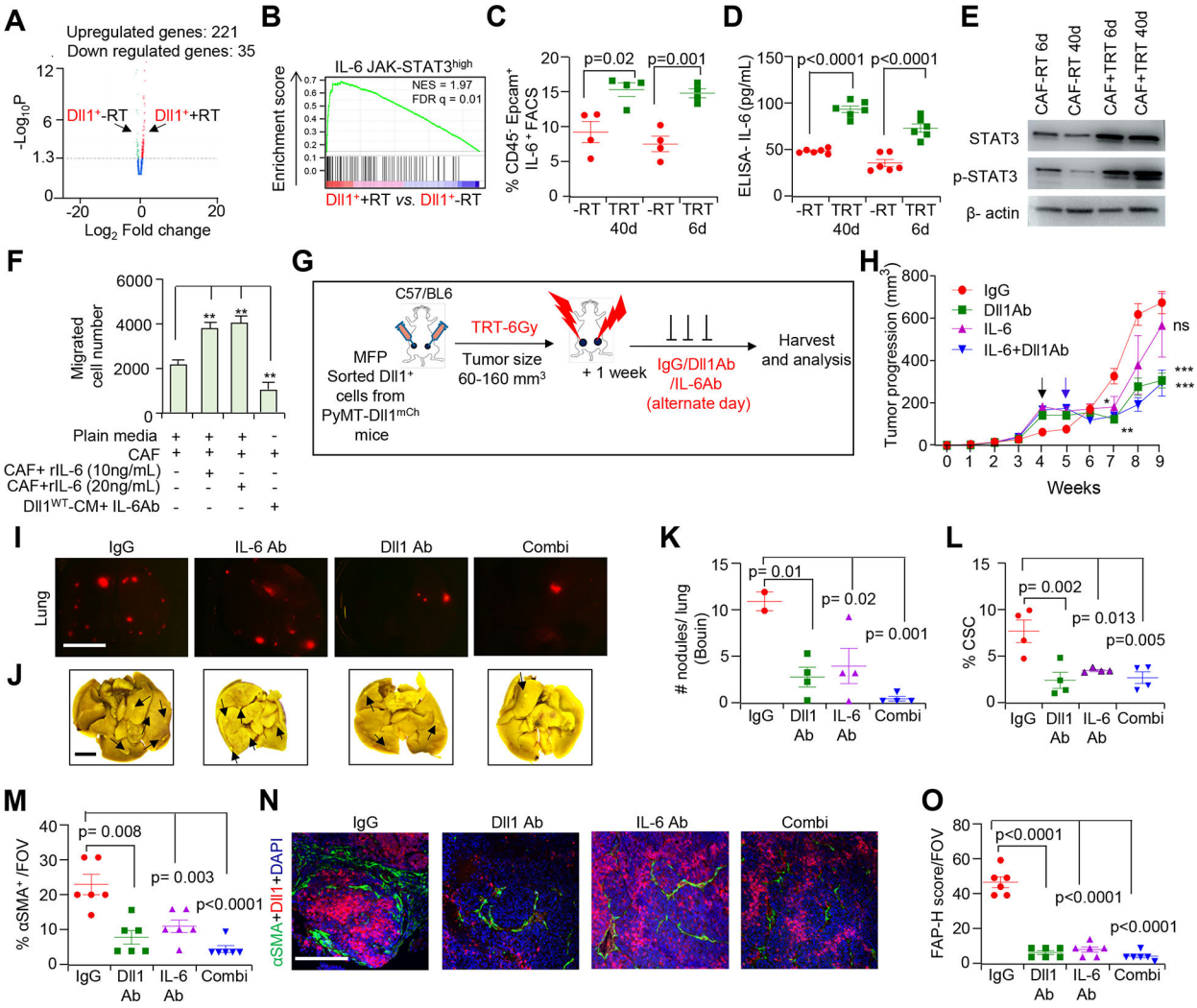

Figure 5.

Dll1 recruits CAFs to the TME in an IL-6 dependent manner during radioresistance and pharmacological blocking of Dll1 and IL-6 antibody sensitizes Dll1$^+$ tumor cells to radiotherapy. **A,** Volcano plot from bulk mRNA-seq depicts enriched peaks for several upregulated genes in +TRT sorted Dll1$^+$ tumor cells upon TRT. **B,** Gene set enrichment analysis (GSEA) demonstrates an enriched IL-6-JAK-STAT3 pathway signature in Dll1$^+$ tumor cells post radiation (TRT). NES, normalized enrichment score and FDR, false discovery rate. **(C** and **D),** FACS plots (**C**) and ELISA (**D**) show higher IL-6 protein levels in Dll1$^+$ tumor cells. **E,** Western blot showing activation of STAT-3 and p-STAT-3 in sorted CAFs from Dll1$^+$ tumors after TRT (Data representative of minimum of two independent experiments). Please see Supplementary Fig. S13 for whole blots. **F,** Bar graphs demonstrate the total number of migrated CD140$^+$/PDGFRα$^+$ CAFs sorted from +TRT Py-Dll1$^+$ tumors (Data representative of minimum of two independent experiments with two technical duplicates). **G,** A total number of 80,000 sorted live Py-Dll1$^+$ tumor cells were transplanted in C57/B6 mice. Schematic model represents *in vivo* treatment of Dll1$^+$ tumors with or without IgG control and anti-Dll1 antibody (18 mg/kg) and anti-IL-6 antibody (20

mg/kg) after a single dose of 6 Gy of TRT. **H,** Tumor growth curves of $Dll1^{+}$ tumors from indicated treatments (n=6 tumors for IgG, n=8 tumors for Dll1Ab and combination group and n=10 tumors for IL-6 group). The black arrow indicates the day when TRT was given, and the blue arrow indicates the day when treatments started. **I,** Representative IF images, **J**, whole lung images and **K**, quantification show $Dll1^{mCh+}$ and metastatic nodules (black arrows show nodules) in whole lungs (n=4 lungs/group). **L,** Scatter plot shows reduced CSC population in anti-Dll1 antibody or IL-6 treated tumors compared to IgG treated tumors. (**M** and **N)**, Quantification and IF of αSMA staining and **O,** quantification of FAP staining in +TRT $Dll1^{+}$ tumors upon indicated *in vivo* treatments. The dots in scatter plot represents field of views (FOVs), n=4 tumors/group. Data are presented as the mean ± SEM. Two-way ANOVA with Bonferroni post-test (**H**), One-way ANOVA with TUKEY post-test (**F, K-M** and **O**) were used to calculate p values. *p<0.05, ** p<0.01; **** p<0.0001. Scale bars, 4 mm (**I** and **J**) and 100 μm (**N**).

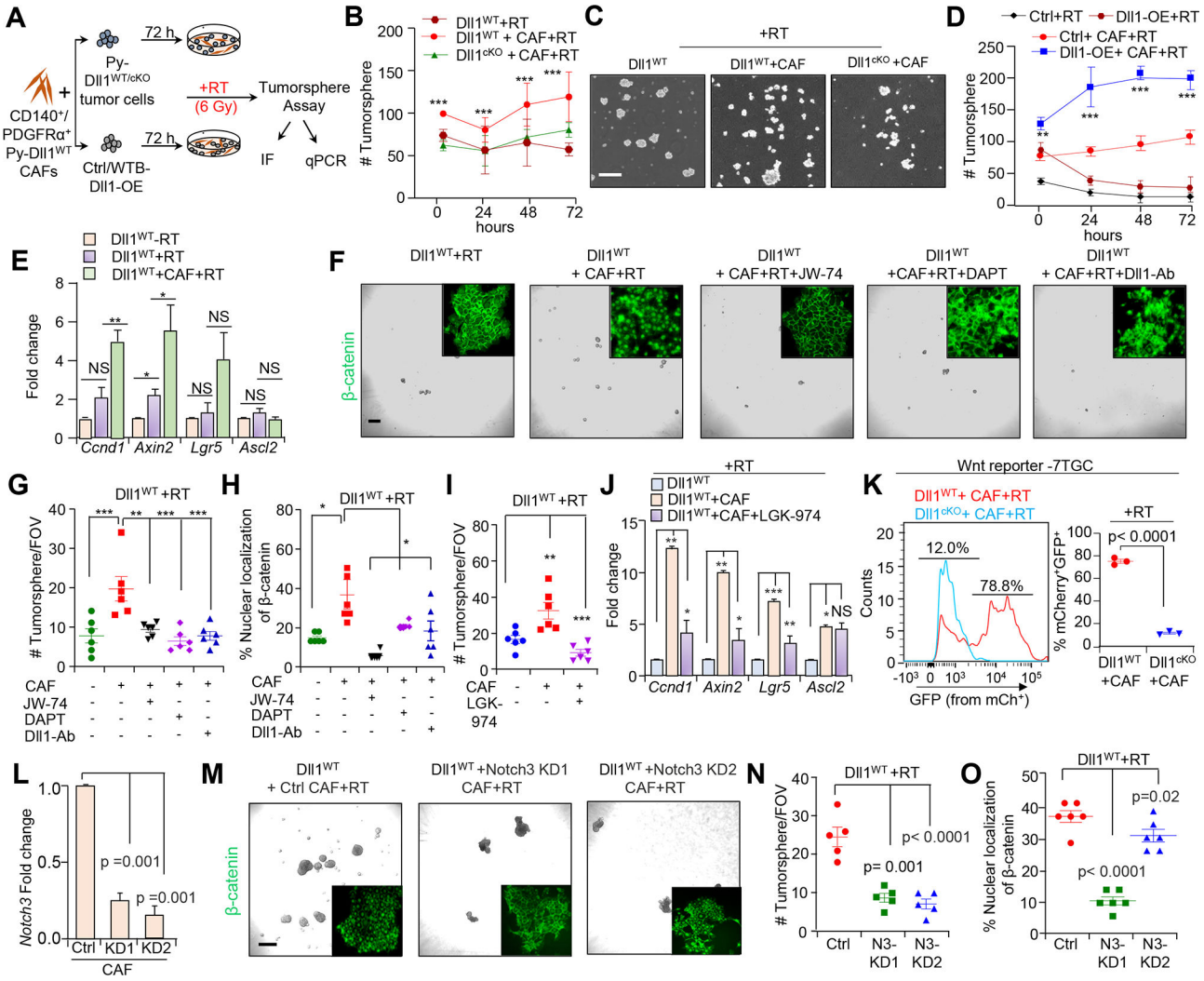

Figure 6.

Dll1-dependent CAFs drive Wnt signaling to promote stemness of Dll1^{+} mouse tumor cells post radiation. **A,** Schematic diagram shows the experimental plan of co-culture of CD140^{+}/ PDGFRα^{+} CAFs. **B,** Line graphs and **C,** representing images showing the number of tumorsphere formed by either Py-Dll1^{WT} or Py-Dll1^{cKO} sorted primary tumor cells co-cultured with sorted WT CAFs post RT. **D,** Line graph shows increased number of tumorsphere formed by Dll1-OE WTB cells when co-cultured with sorted WT CAFs post RT. **E,** qPCR show expression of Wnt signaling downstream target genes (*Ccnd1*, *Axin2*, *Lgr5* and *Ascl2*) in the indicated group. -RT Py-Dll1^{WT} primary tumor cells was considered as a fold change of one. qPCR values were normalized to *Gapdh* (Data representative of minimum of two independent experiments with technical duplicates). **F,** Phase contrast and IF images (insets) and **G**, quantification shows dramatic decrease in the number of tumorspheres derived from CAF co-cultured Py-Dll1^{WT} primary tumor cells after RT in presence of JW-74 (10 μm, pan inhibitor of canonical Wnt signaling) DAPT (200 ng/ml) (Notch inhibitor) or anti-Dll1-blocking antibody (200 ng/ml) compared to untreated cells. **H,** Scatter plots show β-catenin expression in the indicated group. **I,** Scatter plot

demonstrating number of tumorsphere in the indicated group. LGK-974 (10 μm) was used. (Data representative of minimum of two independent experiments with technical duplicates). **J,** Bar graph represents qPCR analysis of decreased Wnt target gens (*Ccnd1, Axin2, Lgr5 and Ascl2*) post RT in $Dll1^{WT}$ primary tumor cell/CAF co-cultures upon treatment with LGK-974 (10 μm) compared to without LGK-974 treated group. **K,** Wnt reporter analysis (**left**) and scatter plot (**right**) show activation of Wnt signaling (based on increase in GFP^{+}/ $mCherry^{+}$ expression) in the indicated group. MCherry expression was used to normalize infectivity of the cells. **L,** qPCR shows stable knockdown of *Notch3* in CAFs. QPCR values were normalized to *Gapdh.* **M,** Representative tumorsphere images and β-catenin IF images (insets), (**N** and **O),** quantification showing tumorsphere number and β-catenin expression in the indicated group. All tumorsphere experiments were repeated twice using technical duplicates. Data are presented as the mean ± SEM. FOV stands for field of view. Two-way ANOVA with Bonferroni post-test adjustment (**B** and **D**), One-way ANOVA with TUKEY post test (**G, H, I, L, N** and **O**) and unpaired student's *t* test **(E, J and K)** were used to calculate p-values. *p<0.05, **p < 0.01, ***p < 0.001. NS- not significant. Scale bars, 500 μm (**C**) and (**F** and **M**; phase contrast) and 100μm (**F** and **M**; insets).

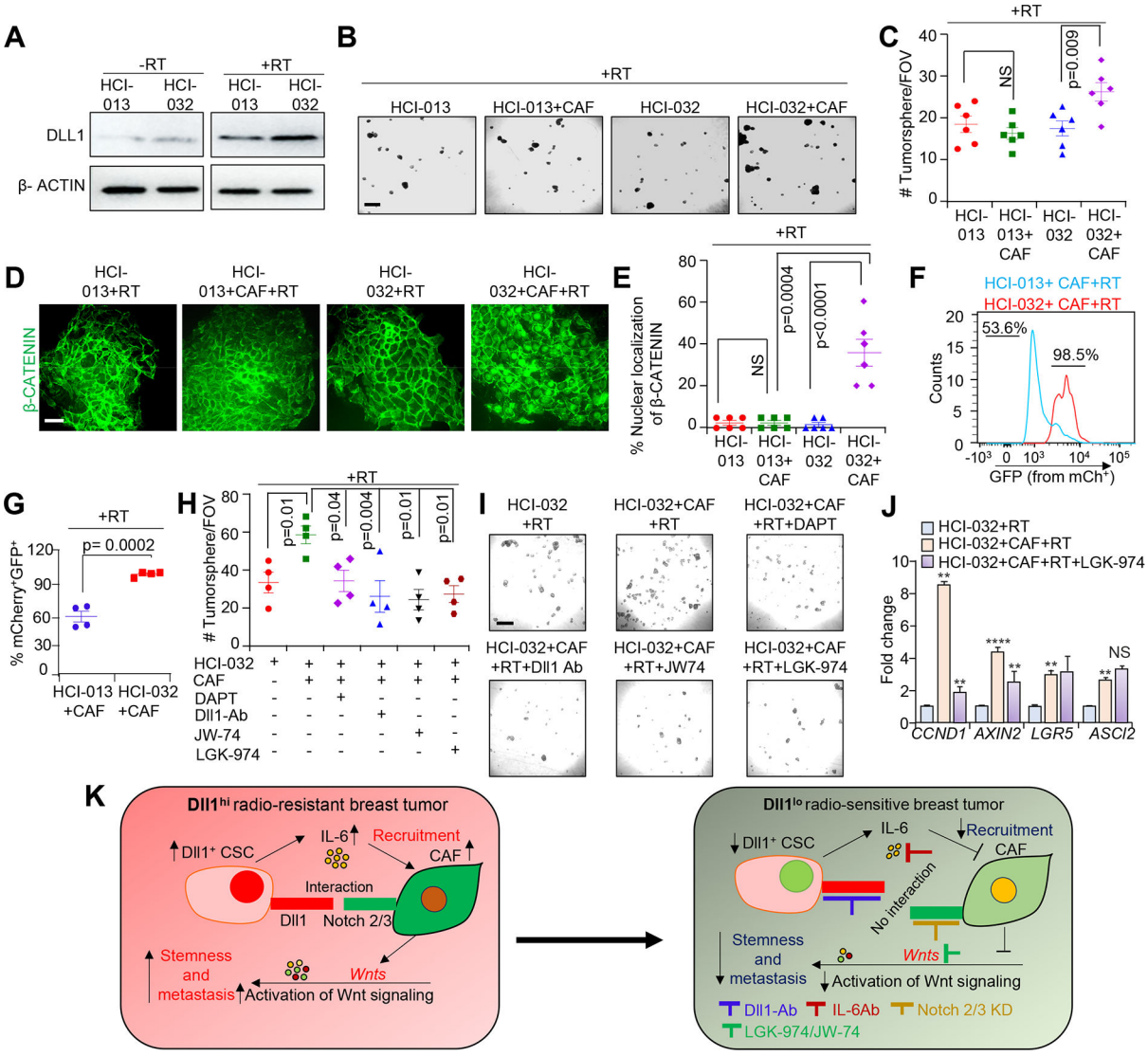

Figure 7.

Pharmacological targeting of Notch signaling or Wnt signaling abrogates crosstalk between CAFs and DLL1^{high} patient derived xenograft (PDX) tumor cells. HCI-013 (radiosensitive) and HCI-032 (radioresistant) luminal non-TNBC ER$^+$/PR$^+$ PDXs, derived from ER$^+$ breast cancer patients were used. **A,** Western blot showing DLL1 protein expression in the indicated PDX before and after RT. Please see Supplementary Fig. S13 for whole blots. (**B** and **C),** Representative tumorsphere images and quantification, (**D** and **E**), representative IF images and quantification showing number of tumorsphere and β-CATENIN expression in the indicated groups. **F** and **G,** Wnt reporter analysis showing increase in activation of Wnt signaling (increase in mCherry$^+$ GFP$^+$ expression) in HCI-032–7TGC PDX cells. **H,** Quantification shows decrease tumorsphere count of HCI-032 tumor cells (co-culture with sorted human CAFs) after treatment with JW74 (10 μM), LGK-974 (10 μm), DAPT, Notch inhibitor (200 ng/ml) or anti-Dll1-blocking antibody (500 μg/mL). **I,** Phase contrast images show tumorsphere images in the indicated group. All tumorsphere experiments were repeated two times using technical duplicates. **J,** qPCR analysis of Wnt target genes from

indicated groups. qPCR data was normalized to *Gapdh*. This experiment was repeated two times using technical duplicates. **K,** Working model showing radiation induced increases in $Dll1^+$ CSC number resulting in IL-6 dependent recruitment of CAFs to the TME. Subsequent Dll1-driven Notch signaling in recruited CAFs induces secretion of Wnt ligands, which activates Wnt signaling in $Dll1^+$ CSCs to enhance radioresistance in breast cancer. Blocking Dll1 and IL-6 or inhibiting Wnt signaling greatly reduces radioresistance in preclinical mouse models. Moreover, genetic ablation of Notch2 and Notch3 receptors in CAFs abrogates Wnt signaling dependent CSC function. Data are presented as the mean ± SEM. Unpaired student's *t* test was used to calculate p values. **p < 0.01; **** p<0.0001. NS=not significant. Scale bars, 500 μm (**B** and **I**) and 100μm (**D**).